Laser Induced Breakdown Spectroscopy (LIBS): Trace level detection in closed contact and at a standoff distance

By:

Fatima Ali Khan
(44-FBAS/MSPHY/F10)

Supervisor:

Dr. ShaistaShahzada

Chairperson,
Assistant Professor,
Department of Physics, FBAS, IIUI

Co-Supervisor:

Dr. Sami ulHaq

Principal scientist,
NILOP Islamabad

Department of Physics
Faculty of Basic and Applied Sciences
International Islamic University, Islamabad

(2012)

INTERNATIONAL ISLAMIC UNIVERSITY

FACULTY OF BASIC AND APPLIED SCIENCES

DEPARTMENT OF PHYSICS

ISLAMABAD PAKISTAN

(2012)

Laser Induced Breakdown Spectroscopy (LIBS): Trace level detection in closed contact and at a standoff distance

By:

Fatima Ali Khan
(44-FBAS/MSPHY/F10)

This thesis is submitted to Department of Physics,

International Islamic University Islamabad for the reward of

MS Physics degree.

Dr. Shaista Shahzada
Chairperson
Department of Physics (FC, FBAS)
International Islamic University
Islamabad

(Chairperson, Department of Physics)

18.4.13

(Dean FBAS, IIU, Islamabad)

International Islamic University, Islamabad

Faculty of Basic and Applied Sciences
Department of Physics

Dated: Jan, 2013

Final Approval

It is certified that the work presented in this thesis entitled "Laser Induced Breakdown Spectroscopy (LIBS): Trace level detection in closed contact and at a standoff distance" by **Fatima Ali Khan**,Registration No. **44-FBAS/MSPHY/F10** is of sufficient standard in scope and quality for the award of degree of MS Physics from International Islamic University, Islamabad.

Committee

External Examiner

Dr. Zafer Iqbal
National Center Physics
Quaid-e-Azam University

Internal Examiner

Dr. Kashif Nadeem
Assistant Professor,
Department of Physics
International Islamic University, Islamabad

Supervisor

Dr.ShaistaShahzada,
Assistant Professor,
Department of Physics
International Islamic University, Islamabad

Co-Supervisor

Dr. Sami Ul Haq
Principal scientist,
NILOP Islamabad

Thesis submitted to

Department of Physics

International Islamic University Islamabad

as a partial fulfillment for the award of the degree of

MS Physics

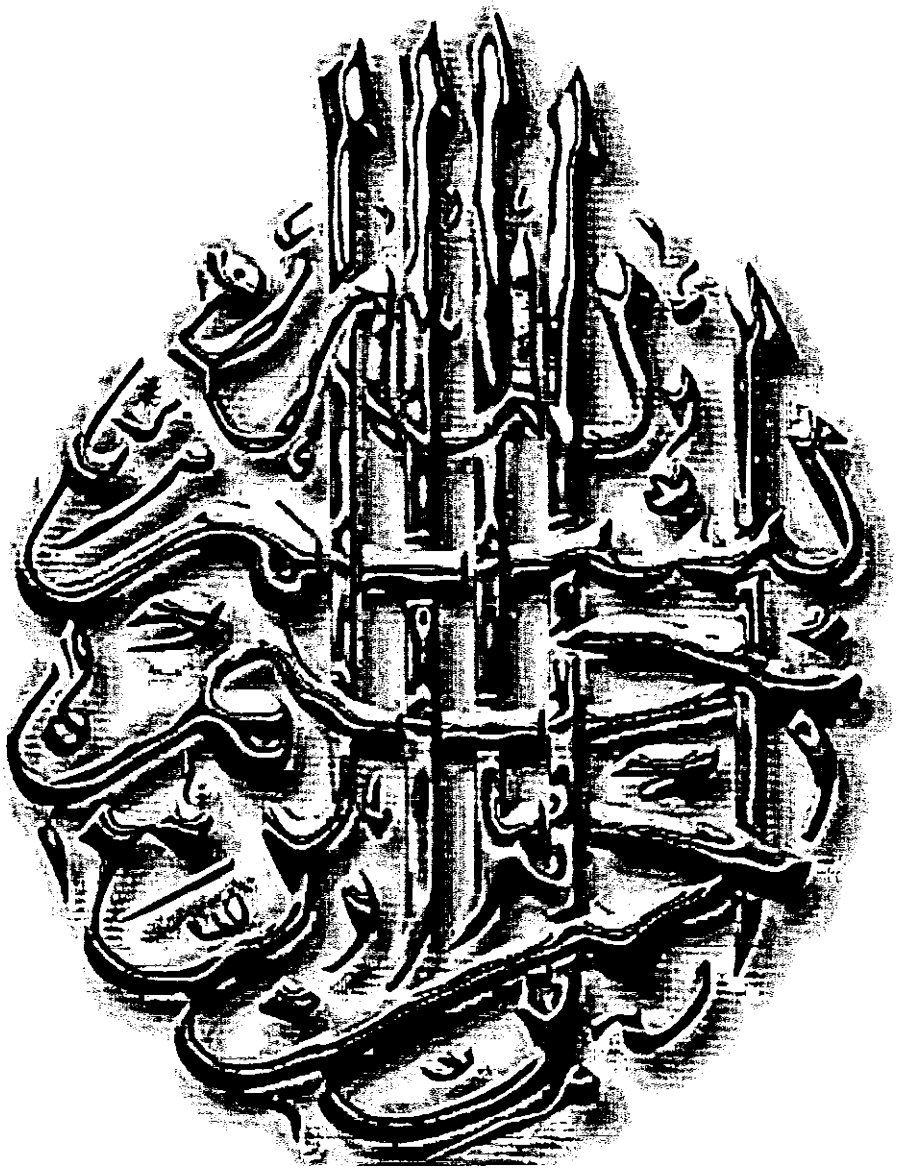

Declaration

I hereby declare that the investigation presented in this thesis work has been carried out by me. The work is original and has not been submitted earlier as a whole or in part for a degree/diploma at this or any other Institution/University.

I also declare that I do understand the terms 'copyright' and 'plagiarism,' and that in case of any copyright violation or plagiarism found in this work, I will be held fully responsible of the consequences of any such violation.

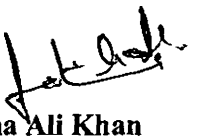

Fatima Ali Khan

(44-FBAS/MSPHY/F10)

Dedicated to;

My Beloved Grandparents, Agha je, Mama, Fadia,

Anum and Noor

Who are a proud of everything that I have done in my life

Acknowledgements

Needless to say, an undertaking such as the preparation of this thesis would not have been possible without Blessings of ALLAH and beloved Prophet Muhammad Sallallaho-alaihe-wassalam and also with the assistance and guidance of many individuals and organizations.

Nevertheless, I would hereby like to express thanks to the following people for their valuable guidance, co-operation and encouragement during the course of my thesis work: My supervisor Dr. Shaista Shahzada for her supervision and her encouragement. It is also indeed a great pleasure to thank my Co supervisor Dr. Sami-ul-Haq for his guidance he showed during my entire work.

I would like to pay my gratitude to Dr. Ali Nadeem who is a source of courage and inspiration for me. Without his extraordinary support it was impossible for me to complete this work in time. I want to especially thank National Institute of Laser and Optronics (NILOP) for providing me best experimental facilities. I would also like to thank Sir Ehsan for his encouragement during my entire MS course work. I also want to thank my friends Palvasha, Hira, Saboohi, Rubab and especially Ghulam Aisha as she has helped me through my hard times. The time spent with you was remarkably fruitful and memorable. I would like to acknowledge my friends Ayesha Tariq and Hina Butt for their love and never ending support.

I have no words to acknowledge the sacrifices, efforts, lot of prayers, guidance, support, encouragement especially of my mother Sumaira raffaqat khan and my Agha je Raffaqat ali khan, your support have made me who I am. To my sisters Fadia, Anum, Noor, Nelum faisal, Shumaila sohail and brothers Sohail khan, Sohail Malik and Faisal mehmood for their genuine and continuos support. Special thanks to my Phupo Abe- Naseem and Dur-e-shehwar for their prayers that have lead me to pursue this degree.

Fatima Ali Khan.

IIUI, Islamabad.

Table of Contents

List of Figures

List of Tables

ABSTRACT

In the present experimental work, laser induced breakdown spectroscopy (LIBS) technique has been used for the trace level detection of aluminum-alloy and steel alloys and organic sample (turnip) in closed contact and at a standoff distance. The emission spectra have been generated using the fundamental harmonic (1064 nm) of the Nd: YAG laser (Neodymium-doped Aluminum Garnet Nd: $Y_3Al_5O_{12}$), and recorded using the LIBS 2500+ broadband (200 - 980 nm) spectrometer having 0.1 nm resolution and equipped with charged coupled device (CCD) detector. We have selected three aluminum alloys Al-alloys ALUSUSSE (412, 413 & 415) and two steel alloys AISI (401,405) with lowest concentration of trace elements. Four trace elements iron, mercury, chromium and zinc (Fe, Hg, Cr and Zn) have been identified from qualitative analysis of the emission spectra of Al-alloy, in which chromium has lowest concentration (0.033%). The qualitative analysis of steel alloys reveals the presence of rich iron emission lines, whereas sulphur, iron, chromium, molybdenum, and nickel was observed as trace elements, in which the molybdenum has lowest concentration (0.002 %). Moreover, the trace level detection has been performed at standoff distance of 2 and 5 m, revealing systematic decrease in signal intensity.

In addition, the organic sample, turnip (*Brassica rapa)* has been analyzed qualitatively using single and double pulse (collinear configuration) LIBS. The trace /heavy elements, such as Fe, Ca, Hg, Zn and Cr have been detected and significant signal enhancement has been observed in case of double pulse configuration. The electron temperature and electron number density were determined using Boltzmann plot method and Stark broadened line profile of iron emission line respectively. Furthermore, the spatial evolution of the emission spectra reveals that the concentration of trace elements increases when moving from center to skin of turnip.

Chapter 1

Introduction

1.1 Laser induced breakdown spectroscopy (LIBS)

The introduction of lasers revolutionized the spectroscopy, particularly the use of pulsed lasers for plasma generation for material analysis. Therefore, the pulsed lasers are useful tool for dissociating materials into their elemental composition and qualitative analysis. Laser Induced Breakdown Spectroscopy (LIBS), is the most important technique used for rapid material analysis. In brief, LIBS, is an optical emission technique in which a high energy laser beam is focused onto the target material. The target material may be in any form such as solid, liquid, gas, and aerosol. As a result of laser matter interaction, luminous plasma with high temperature and electron number density is created. The emissions from this plasma is then analyzed, and characterized spectroscopically to get the information about sample composition, concentration, electron number density, and plasma temperature. Among these parameters, the qualitative analysis of the constituents of sample is rapid and more beneficial as it gives us the on line elemental composition of various samples. In recent years, LIBS has been applied to many areas having particular applications, including the analysis of metals, glass and its elemental composition, nuclear samples, liquids, gases and aerosols and alloys. It has the capability to qualitatively determine the composition of target located at a distance or in extreme environment like high temperature zone or in contaminated areas. The main advantage of LIBS over other analytical methods is that nearly every element in the periodic table can be detected simultaneously with this method. This makes LIBS suitable for rapid on-line analysis, with minimal sample preparation. It has the capability to qualitatively determine the composition of target located at a distance or in extreme environment like high temperature zone or in contaminated areas [1]. During the last decade, LIBS technique has been employed for trace element detection in food items. This application of LIBS is

useful for the assessment and control for healthy alimentation in food products, thus preventing toxic elements from vegetables to be intake by the human body [2].

With the advancement in the field of detectors such as photodiode array (PDA), charge coupled device (CCD) and intensified charge coupled device off detector (ICCD) has revolutionized the LIBS technique for various applications such as standoff detection of trace elements, remote analysis, plasma parameters studies etc. Now-a-days PDA and CCD arrays are used in Echelle and Czerny spectrograph, using PDA and CCD to get spectral information over a wide range can be recorded and ICCDs are used for time-resolved imaging. New areas of study include increasing exploration of vacuum ultraviolet regionof spectrum. Biological applications on human teeth, bones and tissues are becoming more common.

1.2 Historical background of LIBS

Laser induced breakdown spectroscopy (LIBS) is a relatively new technique developed after the first operational of lasers in 1960[3].The earliest experiment of laser induced spark emission was performed in 1960s in which a laser beam produced vapors by irradiating a solid target and the electric spark kept on exciting the ablated plume. The first analytical use of LIBS was reported by Guédon et al. [4] in which the spectrochemical analysis of different surfaces have been performed. Most of the work carried out in those days was related about to the determination of the mechanisms leading to breakdown, measurements of threshold power densities, and investigation of parameters affecting breakdown mechanisms and on breakdown threshold. These experiments are considered as the early age experiments on Laser induced breakdown spectroscopy and after that enormous growth in understanding the physics of the phenomenon has been reported. The affects of various parameters on breakdown threshold such as pulse width [5], spot size [6], and wavelength [7, 8]; have been studied both experimentally and theoretically. Time resolution of the decaying plasma is important to discriminate between spectral features and the continuum light. Various detection systems have been used to obtain temporally resolved spectra, including a streak camera and rotating mirrors. Schroeder et al. [9] devised a method for electronically gating and averaging the signals, a preferred method for time resolution.

Later on gated, intensified charge coupled detectors have been introduced in this field as described in detail in review published by Scott and Strasheim et al. [10]. In early 1980s LIBS began an analytical technique for atomic detection and molecular identification. Applications of LIBS to compositional and qualitative analyses of gases [11], aerosols [12, 13], liquids [14], have been reported. Detection of hazardous gases and vapors in air were important applications worked out during this decade [15,16]. In 1990s the US and some groups in other countries continued their research for making advancements in field of LIBS. Poulain et al. [17] used LIBS to measure the concentration of salt in seawater aerosol droplets and Aguilera and his group[18]detected carbon contents in molten and solid steel samples[19,20].Sandia research group [21] studied the analytical applications of metal emissions from the stacks and developed prototype instrument for monitoring and measurement of toxic metal concentrations. Sabsabi et al. [22] has performed the elemental analysis of aluminum alloys. Work continued on improving the analytical capabilities of the LIBS technique such as Castle et al. [23] studied the factors that influence the accuracy of the technique and Ciuuciand his group[24] applied this technique for quantitative elemental analysis. In the last decade, a rapid and successful application of LIBS has been reported both for qualitative and quantitative analysis in different areas including environmental monitoring [25,26] industrial monitoring [27,28], space exploration [29], biological samples [30], and agricultural materials [31,32,33]. Beldjilali et al [2] evaluate minor element concentrations in potatoes using LIBS. Darwiche et al [34] performed trace detection in solid and molten silicon by using laser induced breakdown spectroscopy. Beldjilali et al [35]. Investigated plasmas produced by using single and double pulses for food analysis.

1.3 Literature Survey

A number of researchers studied different elements for the quantitative analysis so because of some advantages this technique has become more popular in the field of qualitative and quantitative analysis. Here a simple review quantitative analysis of metal alloys (aluminum and steel samples) and soil samples with different elements is given.

1.3.1 Alloys

Sabsabi and Cielo. [22] applied LIBS for the quantitative analysis of trace elements present in the aluminum alloy. Gomba et al. [36] have done qualitative analysis for determination of Al-Li alloys. The experiment was performed in control xenon atmosphere. Dragoff et al. [37] applied time-resolved space integrated LIBS for characterization of Al alloys. Kun et al. [38] carried out quantitative analysis of aluminum alloys in air at atmospheric pressure. Wolfgang et al. [39] determine copper in A533b steel sample. After comparison with atomic absorption spectroscopy (AAS) it was shown that LIBS results at low concentration of Cu are more accurate than AAS. Bassiotis et al. [40] used IR (1064 nm) and UV (355 nm) for production of plasma and recording spectra of steel alloys. Lozep-Moreno et al. [41] studied the elemental composition of low steel alloys using LIBS. Aguilera and his group[18]detected carbon contents in molten and solid steel samples[19, 20]. Shen, et al. [42] detected trace phosphorus in steel.

1.3.2 LIBS on Vegetables

Beldjilali et al. [35] investigate plasmas produced by using single and double pulses for food analysis. During the last decade, LIBS technique has been employed for trace element detection in food items. This application of LIBS is useful for the assessment and control for healthy alimentation in food products, thus preventing toxic elements from vegetables to be intake by the human body[2]. Vincent Juve et al. [43] demonstrated space resolved analysis on fresh potato and carrot.

1.3.3 Double pulse LIBS

Gautier et al. [44] used collinear beam geometry and observe the effects of double pulse on the improvement of sensitivity and reduction of self-absorption. Scaffidi J et al. [45] have used combination of femtosecond and nanosecond laser pulses in double pulse arrangement but in most cases two laser pulses of same wavelength were used. Rai et al. [46] studied emissions through excitation induced by double pulse, experiment performed on liquid. Optimum energy value for the second laser pulse was in the range of 100 to 200mJ to obtain maximum signal intensity. Another important factor that is to be considered is inter-pulse delay.

1.4 Laser Induced plasma

The main properties of laser i.e. intensity, directionality, monochromaticity and coherence distinguish it from any other conventional light source. The laser light emits radiations in continuous wave as well as in short pulses in nanosecond and femtosecond duration. When a short laser pulse strikes the solid target its leading edge causes heating, melting and vaporization into the above layer of the material. The trailing edge of the laser heats the evaporated material, the interaction of the laser with a target surface is considerably modified by the presence of material emitted from the surface by ns laser pulsed irradiation. It exerts a high pressure on the surface and changes the vaporization characteristics of the surface. Since the laser flux density is very high, the ejected material can be heated further by absorption of incoming laser radiation. It becomes thermally ionized and opaque to the incident radiation. The absorbing plasma prevents light from reaching the target surface, which is effectively cut off from the incoming radiation for a large fraction of laser pulse. At the end of the laser pulse, the blow off material becomes so hot that it begins to radiate thermally and some of this radiation may reach the surface, causing further vaporization.

The two main mechanisms in the focal volume of lens in which the peak laser irradiance takes places, predominately occurs i.e.; the multi-photon ionization and the cascade ionization. In cascade breakdown, an electron impacts a neutral atom with enough kinetic energy and ionizes it to eject electron from neutral atom. The energy acquired by initial electron must exceed the ionization energy of the material. The cascade breakdown results in exponential increase of the number density of electrons with time. Multiphoton ionization occurs, when an atom simultaneously absorbs a sufficient number of photons to cause ionization of electron. The rate of photoionization has been expressed as:

$$W^{(n)} = \sigma^{(n)} I^{(n)} \tag{1.1}$$

Where $I^{(n)}$ is the radiation intensity expressed in photon per square centimeter seconds. $\sigma^{(n)}$ is the cross-section of the multiphoton ionization process. Multi-photon ionization takes place at extremely intense laser field with I $\geq 10^{10}$Wcm^{-2}. Despite the very small

cross-section for the multi-photon ionization process, such high laser irradiance is sufficient to produce multi-photon ionization. The process can be represented as:

$$M + mh\nu \rightarrow M^{+} + e^{-} \qquad (1.2)$$

Where M is metal atom, m is no of photons, h is Planks constant, 6.63×10^{-34}Js, ν is the frequency of the photon.Initial electron generation is a problem at higher wavelengths, so neither of the two ways can furnish sufficient number of electrons. At higher intensities, the electric field induced by the laser is capable of pulling electrons from outer orbit. This is what we call initial electron ejection. In the laser field, electron gain energy through inverse electron-neutral bremsstrahlung collisions. Electrons lose energy through elastic and inelastic collisions with neutral particles .Meanwhile, some electrons get lost by attachment, while new electrons are produced through ionization.

1.5 Growth of the laser induced plasma

When short laser pulse strikes the solid target material, it results in its breakdown followed by glow and the ionization of atoms in focal region. This produces plasma consisting of ions and electrons and neutrals, as the number of electrons increases during the plasma growth the plasma reaches a point of breakdown. This level of breakdown is defined as a measure of the electron density of the plasma. In order to breakdown a gas free electrons and sufficient ion and electron densities are needed. First, there must be some initial electrons to "start" the breakdown. These can be generated by the photons in the initial laser pulse. The second requirement for plasma creation is achieving ion and electron densities that can sustain ionization of the gas. In order to achieve this, enough energy must be delivered to the gas. Typical LIBS irradiance is on the order of $10^{8} - 10^{10}$ Wcm^{2}. During the growth of the plasma, electron density is in the range of: $N_e \sim 1^{-10}$ cm^{-3}. As the plasma continues to absorb photons from the laser the electron density grows exponentially. This leads to significant absorption and scattering of the incident laser resulting in fully developed plasma. The goal of LIBS is to identify the material being ablated. To do this we investigate the plasma during the breakdown stage. Ideally, the plasma will be optically thin and in thermodynamically equilibrium. Bremsstrahlung and recombination are free-free and free-bound transitions responsible for a large background

continuum radiation emission in LIBS. Bremsstrahlung occurs when a photon is emitted by electrons that are accelerated or decelerated in collisions. In our case the plasma is heated, and efficiently, via inverse Bremsstrahlung. This means the slow electrons of the plasma interact with the photons, **equation (1.3),** to generate fast electrons. Once there is sufficient kinetic energy in the electrons they collide with other atoms, knocking off more electrons and creating more ions and more free electrons. This exponential increase in electrons is called avalanche or cascading, it occurs during the laser pulse. Afterward, as the plasma cools, the ions start to fall back into neutral atoms. This is the continuum radiation (free bound). The electrons in the plasma slow down generating bremsstrahlung radiation. These two sources are the broadband background radiation we see at short delay times (but after the laser pulse is finished).

$$e^{-}(slow) + h\nu \rightarrow e^{-}(fast) \tag{1.3}$$

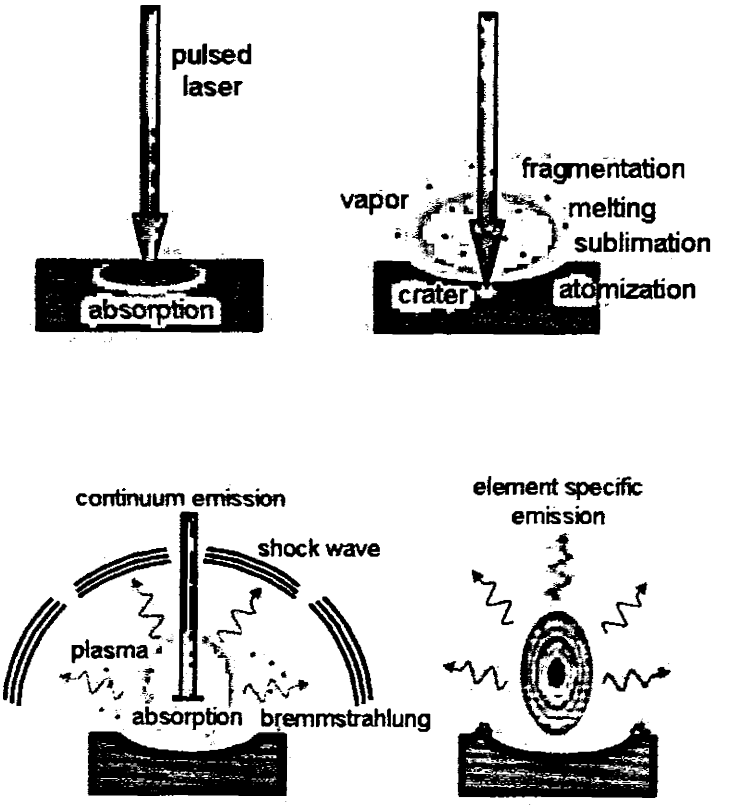

Figure 1.1 A summary of laser ablation processes and various mechanisms occurring during each process.

When an atom absorbs a photon it absorbs its energy and the electrons are pushed to a higher energy state. The energy of the photon, hυ, allows the electron to move from E_1 to E_2. Ionization of the plasma is a function of time; ionization is higher at early stage plasma of the plasma formation.

Where,

$$E_2 - E_1 = h\nu \tag{1.4}$$

Let M be a neutral atom .then cascade breakdown can be described as follows:

$$M + e^- \rightarrow M^+ + 2e^- \tag{1.5}$$

Where M is metal atom, m is no of photons, h is Planks constant, 6.63×10^{-34}Js, ν is the frequency of the photon.

1.6 Temporal history of LIBS Plasma

Time resolution of the plasma light in LIBS allows for discrimination in favor of the region where the signals of interests predominate. It is necessary to temporally gate the detector because the delay between the continuum emission of radiation and characteristic radiation is in the order of 10 μs. Plasma cools and decays, during these decay constituents (ions and electrons) give up their energies through recombination resulting neutral and then molecules. A schematic diagram of temporal history of LIBS plasma initiated by single laser pulse is shown in **Fig. 1.2**.

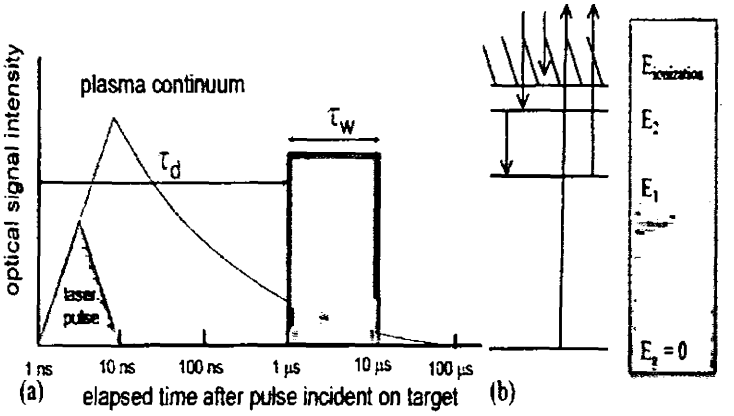

Figure 1.2(a) Schematic overview of temporal history of LIBS plasma. (b) From left to right bound-bound; free bound; free-free; ionization from ground state; ionization from an excited state.

The **Fig. 1.2 (a)** is an overview of the temporal history of single laser pulse initiated LIBS plasma, which plots the optical intensity emitted by the plasma as a function of time after the initiation of laser pulse. Where t_d is the delay from the initiation of the laser to the opening of the window during which signal will be accepted; and t_w is the length of the window. There are highly ionized and neutral atoms present in the laser induced plasma. The highly ionized species are observed close to the plasma plume and lines of lower ionization are observed close to the outer region of the plasma plume. The neutral atomic emission dominates after the plasma has expanded. The time variation of spectral line intensities indicates that highest ionized states are present at early stage of plasma and lower ionized states appear at later stage. At early stage, plasma is highly ionized, at later stage, the electron-ion recombination takes place and neutrals atoms and molecules are formed. All the way during the laser induced plasma, a background and continuum exists that decays quickly with time. This continuum is usually due to the bremsstrahlung (free-free transitions) and recombination (free-bond transitions).In bremsstrahlung process photons are emitted during the acceleration and deceleration of electron. During the recombination free electron is captured into an ionic and atomic energy level and gives up its kinetic energy in the form of a photon. **Fig. 1.2 (b)** shows the typical plasma radiation processes. Where E is energy in joules, the frequency, wave number and wavelength of a transition are given by:

$$\upsilon = \Delta E/h, \qquad \nu = c/\lambda \tag{1.6}$$

ΔE is the energy level difference. Energy levels are conventionally listed with the ground state as zero.

1.7 Factors affecting LIBS

Laser parameters, physical, chemical and mechanical properties of the sample and ambient conditions are the main factors that can affect signal intensities and LIBS measurements.

1.7.1 Laser parameters

The evolution of plasma is mainly dependent on parameters such as laser intensity, wavelength and size of focus spot. These parameters can affect LIBS emission spectra to

a great extent. For the generation of plasma the laser irradiance must be greater than the threshold value which is several Wcm^{-2} for a nanosecond laser pulse. At longer wavelengths, the dominant ionization mechanism is collision-induced ionization, whereas at shorter wavelengths photoionization takes over the dominance. Electron temperature is maximum for the longer wavelengths but minimum value of number density are obtained at the same irradiance, this results in low value of mass ablation rate for longer wavelengths but maximum at shorter wavelengths. Pulse width is another prime factor which influences the LIBS measurements. Dissipation of thermal energy is much less for shorter pulses, which leads to the enhanced mass ablation.

1.7.2 Physical properties of sample

LIBS can be applied to all types of materials without any sampling process. But the physical properties of the sample which can be influential are reflectivity of the target material, specific heat, melting and boiling point, and density. The amount of laser energy absorbed by the target surface is determined by its surface reflectivity. The laser energy causes heating of the sample, due to which phase change of sample occurs and hence reduces the reflectivity and increases the material ablation. The quantity of the material vaporized depends on the properties such as thermal conductivity, specific heat and boiling point of the sample. When thermal conductivity is high, amount of material vaporized is low.

1.7.3 Ambient Conditions

The ambient conditions affect the dynamics of the plasma plume and also emission characteristics and confinement of the plasma. The plasma interacts with the surrounding gas results in expansion of high-pressure vapor. A shock wave is generated which transfers the heat to the surroundings. The breakdown threshold value also depends on ambient conditions.

1.8 Optical thickness and Self-absorption in LIBS plasma

The main objective of LIBS plasma is to generate optically thin plasma, free from self-absorption and is in local thermodynamic equilibrium (LTE) and having the same elemental composition as that of the sample.

1.8.1 Optically thin plasma

The plasma is optically thin when the emitted radiations traverses and escapes from the plasma without considerable absorption and scattering. During the entire observation interval, the LTE conditions are assumed to be true. The intensity of the emitted radiation is given by;

$$I(\lambda) = \left[\varepsilon(\lambda) / \alpha(\lambda)\right] \left\{1 - exp\left(-\alpha(\lambda) L\right)\right\} \quad (1.7)$$

Where ε (λ) is the emissivity, α (λ) is the absorption coefficient (cm), and L is the plasma length along the line of sight to the observer. When α is so small then the above equation can be written as

$$I(\lambda) = \left[\varepsilon(\lambda) / \alpha(\lambda)\right] \left[\alpha(\lambda) L\right] \approx \varepsilon(\lambda) L \quad (1.8)$$

This is condition for plasma to be optically thin, for evaluating the plasma parameters and extracting qualitative data from the line intensities it is essential to confirm that the plasma is not optically thick. If plasma is optically thin, self-absorption effects are not observed in the emission spectra. If plasma density is very high, the plasma itself absorbs its own radiations and the relative intensities will depart from the intensity rules. The resonance lines or the most intense lines approach a flat-topped. In extreme cases, a self-reversal may occur which causes a dip at the central of the line.

1.8.2 Local Thermodynamic Equilibrium (LTE)

The most important thing for plasma studies is that plasma should be in local thermodynamic equilibrium. The condition for LTE is that the collisional processes must dominate over the radiative so that there would be no shortage of radiative energy. If we become more precise then we can say that in excited state de-excitation through collisions must be higher as compared to one resulted from spontaneous radiation. This is the essential condition requiring a high electron density to establish LTE. An elaborated discussion has been available in "Laser induced breakdown spectroscopy". The simplest way to verify the existence of LTE is by using the McWhirter criterion, i.e. the lower limit of electron number density for which the plasma will be in LTE is expressed as:

$$N_e \geq 1.6\times10^{12} T_e^{\frac{1}{2}} (\Delta E)^3 \, cm^{-3}, \quad (1.9)$$

Where T_e is temperature in K and $\Delta E(eV)$ is the largest energy gap for which the condition holds.

1.9 Qualitative analysis

One of the most promising applications of LIBS atomic emission spectra is the identification of elements present in the source of light (plasma emission).Qualitative analysis reveals the presence of a given element present in the sample or presence of multi-elements can also be done by the qualitative analysis. For the qualitative or quantitative analysis the basic requirement of any LIBS measurement is the emission spectra recorded from a single pulse. The basis of any LIBS measurement is the plasma spectrum which has information about the elements present in the target sample. This information is in the emission lines located at specific wavelengths, the intensity of the lines and in the relative intensities of the lines. This information is important for analyzing the sample.

The use of this technique for qualitative analysis of samples which emit characteristic light (yellow for Na, red for Ca) when subjected to a high energy laser beam, dates back to Bunsen and Kirchoff in 19th century. Major advancements in astrophysics are the results from the studies of the spectra of the emissions from the radiating stellar bodies which have provided information about their chemical composition. Some elements are excited easily so that their emission spectra can be observed and recorded, than others. Non-metal atoms are more difficult to excite as compared to metal atoms because of their high ionization potential. It is found that presence of easily excited atoms in a sample, suppress the emission from atoms that are comparably difficult to excite. Thus emission from helium would be suppressed in the presence of nitrogen, same with the nitrogen in presence of mercury and that of mercury is suppressed if the sample contains potassium. When a sample is placed in an arc or discharge source and atoms present in the sample get excited, a large number of lines with varying intensities are observed covering a wide range of the spectrum. As one dilutes the amount of the element present in sample, the number of observable lines is reduced and ultimately only a few lines of that element

remain observable. These lines are termed as persistent lines. It has been found that the persistent lines are the lines of maximum intensity. From this description of the persistent lines it is apparent that in the qualitative analysis for a specific element we need to consider only for the persistent lines of that element.

The plasma spectrum maybe used to identify the constituents and their concentrations, by a suitable wavelength and intensity calibration methodology.

The intensity of an emission line in the plasma is given by:

$$I = \frac{1}{4\pi} A_{ip} h\upsilon_{ip} N_p \tag{1.10}$$

Where I is the intensity of the emission line, υ is the frequency of the transition from state p→i

A_{ip} is the Einstein coefficient for spontaneous emission,

N_p is the population of the high energy level,

h is the plank's constant.

$$\frac{N_p}{N_0} = \frac{g_p}{g_0} e^{-(E_p - E_0)/KT} \tag{1.11}$$

Moreover, the Boltzmann population distribution is given by:

$$N_p = N_o \frac{g_p}{Z(T)} exp\ (-\frac{E_p}{KT}) \tag{1.12}$$

N_o is the density of emitted species, g_p the degeneracy of the higher level, Z the partition function, E_p the energy of the higher level and T the excitation temperature. Thus replacing the N_p in **eq. (1.10)** with the Boltzmann distribution in **eq. (1.12),** the emission line intensity is directly proportional to element concentration.

$$I = \frac{1}{4\pi} A_{ip} h\nu_{ip} N_o \frac{g_u e^{-E_u/KT}}{Z(J)} \tag{1.13}$$

According to **eq. (1.12),** one can determine the population density of the relevant species (atoms or ions) for an element in plasma from a measurement of the absolute intensity of corresponding transition and knowledge of the excitation temperature and atomic constants. However, it is not possible to derive a theoretical expression relating N and concentration of that element in solid sample under investigation. Hence, in practice, an

empirical relation is sought between the observed line intensity (I) and corresponding concentration (C) i.e.

$$I = F(C) \tag{1.14}$$

Here F (C) is called analyte calibration function and the graph between the LIBS intensity of a line of specific element and the concentration is called calibration curve. Such curve can be drawn by measurement of reference samples of known concentrations termed as standard samples and can be used to determine the elemental concentration in unknown sample.

In search for a definite element, the identification of the persistent lines should be sufficient to confirm the presence of the element. The identification of unknown elements requires a more complete identification of all spectral lines in the emission spectrum of the sample. After this procedure of identification, the remaining unidentified lines are generally weak and they may be up till then unobserved lines of the major constituents or can be lines of the unknown minor constituents or can be described as trace elements. Tables of persistent lines of many elements are present in a book by Brode and also in a publication by Meggers[47]. In most cases of qualitative analysis, the major constituents of the sample are mostly determined by inspection of the lines of maximum intensity and other lines of these constituents can be identified by use of the tabulation of spectral lines of the elements [47, 48]. After this procedure of identification, left unidentified lines are generally weak and they may be up till then unobserved lines of the major constituents or can be lines of the unknown minor constituents or can be described as trace elements. In the case of trace elements, the lines must be among the stronger lines of these elements. The unknown element can then be identified by comparison of these lines with the persistent lines of other major constituents of the sample.

1.10 Factors affecting the Qualitative analysis

1.10.1 Sample Homogeneity

This is technique for a direct consequence of no sample preparation and mostly affects the analysis of solids. Preparation typically produces a homogeneous sample; the lack of preparation complicates the analysis of non-homogeneous samples with a point detection

method such as LIBS. The area interrogated is small, typically 0.1 – 1 mm diameter, involving a very small mass of material. Non-uniformities may be averaged out using a number of laser plasmas to repetitively interrogate different areas of a sample and the results are combined to produce an average measurement

1.10.2 Matrix Effects

Chemical composition and surrounding environment of the targeted sample can affect the emission intensity of a line in an unpredictable manner. The effect of host elements on the analyte during LIBS plasma reaction is called matrix effect. Matrix effects are adverse host influence on LIBS resulting in inconsistent line spectrum intensity due to chemical composition and material properties. With each laser shot on target material, the analyte changed via reactions with its surroundings. Matrix effects can be divided into two categories, physical and chemical effects. Differences between specific heat, thermal conductivity, heat of vaporization, absorption at the laser wavelength, and particle size contribute to the occurrence of physical matrix effects. Chemical matrix effects reveal their occurrence when the presence of one element has an effect on the emission of another element. For example, easily ionizable species increase the electron density, therefore reducing the intensity of less ionizable components.

1.10.3 Sampling Geometry

The geometrical shape of the plasma and spatial emission intensity profile are strongly dependent on the laser power density and on parameters such as optical alignment for laser focusing and collection of emissions the emission from plasma plume for recording the spectrum. Therefore, LIBS signal is dependent on the optical alignment and collection of emitted light for recording the spectrum.

1.10.4 Relative intensities of the emission line from wavelength tables

Qualitative analysis with LIBS begins with the identification of the stronger emission lines provided by LIBS spectra. In addition, one may also search out a material's LIBS spectra for the presence of specific lines associated with elements of prior interest. Various references for atomic line spectra wavelength and relative intensity can be found in the general literature. ARL and the NIST (U. S. National Institute of Standards and

Technology) provide line spectra public data bases on the World Wide Web [50, 51]. These web sites include reliable LIBS research tools that are informative, easy to access and utilize. The ARL site includes only the stronger emission lines for 72 elements referenced from LIBS technical publications. The NIST site is more comprehensive and includes both weak and strong emission lines for over 100 elements referenced from various atomic line emission spectroscopy references. Wavelength resolutions of 0.03nm to 0.2nm are common and often appropriate for identification of a major element by a strong line emission.

1.10.5 The ionization stage of the element

If two elements are likely to be found in a sample in an equal manner, if their lines spectrally interfere and one line corresponds to a neutral species and the other one belongs to a doubly or triply ionized species, it is most likely that the line should be assigned to the neutral species. Although once-ionized that is neutral species are often observed in LIBS plasma, the observation of higher ionization stages is unlikely to be found in air. The lines with ionization potentials of 6 eV or less are more likely to be observed whereas species having ionization potential to >10eV, their presence is unlikely to be observed.

1.10.6 Optimization of LIBS working conditions

Working conditions were optimized by considering the net emission line intensity magnitude and the signal to background ratio as optimization criteria. For the single pulse mode, the laser energy and the delay time are the most significant working parameters to be optimized. For the double pulse mode additional parameters have to be taken into consideration such as the pulse energy of the second laser and the inter-pulse separation.

1.10.7 Condition of surface

The factor that affects entire LIBS measurements, even the simplest identification of elements in a target sample, is the condition of the surface. LIBS is a surface analysis technique, though repetitive laser shots at the same location can be used to ablate the surface and reach to underlying layers. Surface detection is a useful in some applications, however, for example, to detect stains on a surface where large mass in present because

of the underlying substrate. Other analytical methods which are capable of penetrating through the surface layer (e.g. x-ray fluorescence) to sample a large volume of the substrate composition would be required to monitor a small signal from a thin layer of surface, on the top of a large signal from the bulk sample. whereas, repetitive ablation at the same focus point can be applied to ablate through a thin weathered layer on a rock ($\sim 100 \mu m$ thick) to record changes in composition as the underlying bulk rock is approached.

1.11 Identification of emission spectra

The emission spectra have been analyzed using the electric dipole transition selection rules. For an electric dipole transition, to take place, the matrix element of the electric dipole moment operator shall be non-vanishing.

$$\langle n'l'm_l' | -er | nlm_l \rangle \tag{1.15}$$

The only transitions between states of opposite parity are allowed for electric dipole transitions, because the electric dipole matrix elements of **eq. (1.15)** will vanish unless$\Delta l = \pm 1$.

$$\Delta S = 0, \tag{1.16}$$

$$\Delta L = 0 \pm 1 \ (L = 0 \nrightarrow L = 0), \tag{1.17}$$

$$\Delta J = 0 \pm 1 \left(J = 0 \nmapsto J = 0 \right), \tag{1.18}$$

These rules depend on validity of L-S coupling scheme, and $\Delta S = 0$ does not hold for the heavier elements in which the inter-combination lines of different multiplicity can be quite strong.

1.12 Stand-off detection of LIBS

Stand-off techniques have gained attention as valuable methods for material analysis at remote distances. This technique is applicable when looking at hazardous contaminants in the environment or residual explosive material, where it is required for the analyst to remain at a safe distance from the material being investigated. In the Stand-off technique

the laser beam is directed along an open path (through air, gas or vacuum) towards the target to generate plasma and then emission is collected at a distance. Open path LIBS with stand-off arrangements are mainly used with nanosecond laser pulses. The distances achievable depend on the method of generating plasma (conventional focusing using a combination of lens or mirror system) and on the method of collection of the plasma light. Even though robust plasma may be formed, sufficient light must be collected to observe a useful spectrum. This method needs optimization of laser, optics and detection system performance.

1.12.1 Advantages of remote LIBS

- Ability to analyze targets located in environments where access by personnel and/or non-disposable equipment is confined (e.g. areas contaminated by toxic, radioactive materials or a confined area).
- Ability to process control where analysis must be done rapidly and from a distance (e.g. molten metals and glasses).
- Applied for analysis of physically inaccessible targets (e.g. geological features on cliff faces).
- Investigation of targets located in hazardous environments where any physical access is not possible but optical access is possible (e.g. through a window on a glove box).
- Rapid analysis of distinct widely separated targets from a single point.
- Screening of large surfaces by scanning laser pulses along a surface.
- There is no possibility of damaging or contamination of equipment by locally harsh.

Environments Among all the remote LIBS techniques, open path LIBS is of particular interest because measurements can be carried out in a truly 'stand-off' mode without any invasion into the sample region. The only condition is line-of-sight optical access.

1.13 Double pulse configuration

The main limitation of the LIBS is its low sensitivity and precision as compared to several atomic emission spectroscopic techniques. In order to improve the LIBS emission intensity, several approaches were suggested. One of the approaches is the double pulse configuration.

- **Collinear Configuration:** In collinear configuration, the two laser pulses propagate along the same axis and are both directed to the target surface. In this configuration, the first laser beam produces the plasma then the second laser pulse arrives with some inter-pulse delay causing reheating of the plasma produced by the first laser. This plasma evolves in a rarified gas atmosphere enclosed by the shock wave produced by the first laser pulse.
- **Orthogonal Configuration:** In the orthogonal beam geometry, the first laser beam irradiates parallel to the target surface generating the plasma above the target surface and the second pulse (ablative) is directed orthogonal to the target. This approach is also very effective for the enhancement of emission signal intensity.

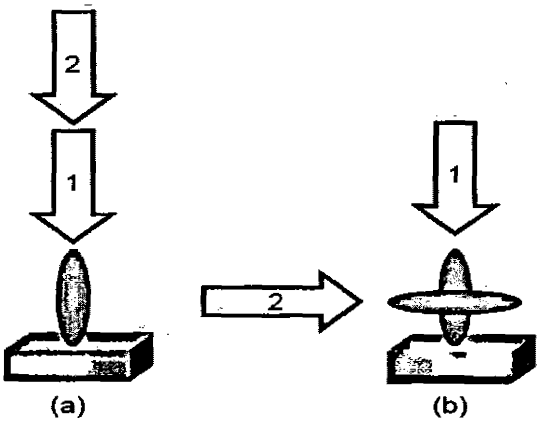

Figure 1.3Commonly used beam geometries for dual-pulse LIBS. (a) Collinear dual-pulse arrangement, wherein both pulses are focused upon the same point on the sample. (b) Orthogonal reheating configuration, for which an air spark is formed after ablation.

As shown in **Fig. 1.3** two laser pulses are required in either collinear or orthogonal configuration. The inter-pulse delay is ranging from picoseconds up to few microseconds to generate the plasma. The increase in the signal intensities in double pulse LIBS is due to the better coupling of laser energy to the target and ablated material, leading to more atoms in excited state and increased rate of ablation, plasma volume, ion density and plasma temperature, plume expansion velocity, lifetime of the plasma. This also improves the lower limits of detection of different chemical elements by one or two orders of magnitude. From the experimental point of view, the collinear configuration is the

simplest approach for double pulse LIBS. This configuration was first investigated by Cremers et al. [52]; provide spectrochemical analysis of liquids using the laser. Gautier et al. [44] has proved that double-pulse has capability to enhance the intensity of signal by more than one order of magnitude while analyzing aluminum samples.

Collinear dual-pulse LIBS is used in many experiments explains emission increases in through a combination of increased material ablation, an increased plasma volume, reheating of plasma by the second pulse. An orthogonal beam orientation has also employed in many cases, Uebbing et al. [53] described reheating of a laser plasma by a 2^{nd} laser pulse **Fig 1.3 (b)**,where the second laser pulse is focused in parallel direction to the target surface and reheat or re-excite material ablated by the first laser. Different combination of wavelengths has also been observed. Scaffidi et al. [45] have used combination of femtosecond and nanosecond laser pulses in double pulse arrangement but in most cases two laser pulses of same wavelength were used.Rai et al. [46] studied emissions through excitation induced by double pulse, experiment performed on liquid. Optimum energy value for the second laser pulse was in the range of 100 to 200mJ to obtain maximum signal intensity .Another important factor that is to be considered is inter-pulse delay. Inter-pulse delay ranges from picoseconds up to few microseconds can be used to generate the plasma. Rizwan et al. [54] have demonstrated optimization of interpulse delay at aluminum samples. The optimum value of the inter pulse delay observed to be dependent on the sample material. Kuwako et al. [55] performed detection of sodium in water through double pulse laser.

Chapter No. 2

Experimental setup and Procedure

In this chapter, the experimental setup and procedure to record the emission spectra of metal alloys and soil samples have been described.

- Two Nd: YAG laser system (Spectra Physics, USA).
  - i) PRO- 230 (30 Hz, 10 ns)
  - ii) DCR-3 (10 Hz, 7-9 ns)
- Seven channel high resolution LIBS 2500+ spectrometer (Ocean Optics, USA).
- Sample chamber and sample holder.
- Sending telescope and Receiving telescope (Newtonian telescope).

2.1 Laser Systems

Various Laser systems have been used for plasma generation, depending on their power, pulse duration. The radiation emitted from the laser either continuous or in short pulses, but in laser induced breakdown spectroscopy (LIBS), mostly pulsed lasers are used. For laser system, it is important that the laser should have enough irradiance to generate plasma on the surface of the target. The lasers systems used in LIBS include solid state lasers, like the Nd: YAG, Ruby laser, femtosecond lasers and gas lasers such as Excimer lasers, CO_2 lasers etc. In the present experiments, Nd: YAG laser have been used to generate plasma of alloys and soil samples.

2.1.1 Nd:YAG laser

We have used Q-switched Nd: YAG laser system (Spectra Physics) for our experiment having pulse duration of the order of 10 ns and 10 Hz rep. rate The Nd:YAG laser is most widely used in laser induced Breakdown spectroscopy(LIBS) due to applications because of their reliability, easy to handle source of laser pulses together with high irradiances [1] and its compact form. The Nd: YAG laser is a flash lamp pumped, solid state laser with

fundamental output at 1064 nm and other at 532, 355 and 266 nm. Second, third and fourth harmonics can be produced using non-linear crystals.

The Nd: YAG (Neodymium-doped Aluminum Garnet Nd: $Y_3Al_5O_{12}$) crystal used as lasing medium in solid state lasers. Nd^{+3} act as the active medium. The crystalline YAG host is doped with about 1% neodymium by atomic percentage. The pumping source to excite the atoms can be discharge source, flash lamps or laser diodes. As shown in **Fig. 2.1**, the Nd: YAG laser is a four-level laser system in which the atoms are excited from ground state ($^4I_{9/2}$) to the $^4F_{5/2}$ state and from there, the atoms decay non- radiatively to the $^4F_{3/2}$ state having life time about 230 μsec.

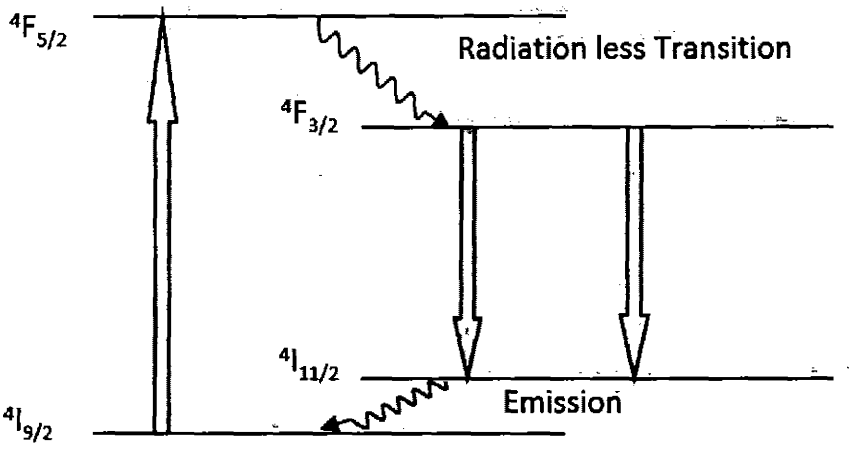

Figure 2.1 Energy level diagram of Nd: YAG laser

Among other possible transitions from this state, the most probable lasing transition is the $^4F_{3/2} \rightarrow {}^4I_{11/2}$, because this transition has maximum stimulated emission cross section and low lasing threshold. As a result, photons at 1064 nm are emitted and the Nd atoms relax back to the ground state. This process is repeated each time when flash lamp fires; and a Q-Switch is used to shorten these pulses up to nano-second and to raise the peak power of the output laser pulse. The switching of the laser pulses are fixed to 30 Hz (PRO-230) when triggered internally.In the present experiments, we have used two different Nd: YAG lasers, the Spectra Physics (PRO-230 and DCR-3). The necessary specification of these laser systems are listed in Table 2.1.

Table 2.1 Specifications of Nd: YAG laser

Specifications	*Nd: YAG (DCR-3)*	*Nd: YAG (PRO-230)*
Energy per pulse (mJ)	*850*	*1000*
Pulse Width (ns)	*7-9 ns*	*10 ns*
Line Width	*1.0 cm^{-1}*	*1.0 cm^{-1}*
Beam Divergence	*> 0.5 m rad*	*> 0.5 m rad*
Rep. Rate (Hz)	*10*	*30*

2.2 LIBS-Spectrometer

A 7-channel LIBS spectrometer (LIBS 2500+, Ocean Optics, USA) is used in the present experiments. It's a detection system having capability of real time qualitative analysis of trace elements. It consists of seven high resolution HR 4000 miniature spectrometers covering the spectral range from 200 to 980 nm with spectral resolution 0.1 nm (FWHM). Each spectrometer is coupled with 2048-element linear CCD array. All the seven spectrometers are triggered simultaneously to acquire and read out data simultaneously and are lumped together as shown in **Fig.2.2**. As a result of laser matter interaction, plasma is generated and the emissions are collected and transmitted to LIBS2500+ via multi-mode fiber cable. The application software "OOILIBSplus" provided with LIBS 2500+ set up is used to operate and control of laser firing and to save and analysis the emission spectra.

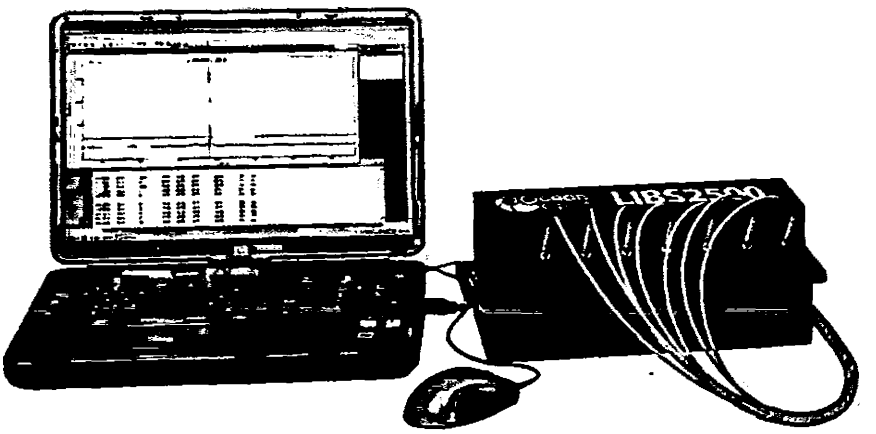

Figure 2.2The LIBS2500 plus set up is built around HR4000 high resolution miniature spectrometer.

2.2.1 HR 4000 Spectrometer

The LIBS2500+ is based on high resolution miniature fiber optic HR4000 spectrometers. The HR4000 spectrometer is based on Czerny Turner configuration. The working principle of this configuration is shown in **Fig. 2.3**. The light from the plasma enters into the housing via entrance slit and arrives at the collimating mirror, which collimates the light and direct to the grating. Grating disperses the light at different angle according to their wavelength and then falls on the focusing mirror. The resolution of each spectrometer depends on the grating fixed inside with respect to the wavelength range. A detector based on linear array (CCD) detects the light and convert it the optical signal into digital signal that is transmitted to spectrometer software for further analysis. Each HR 4000 spectrometer comprises the following parts, which are described below;

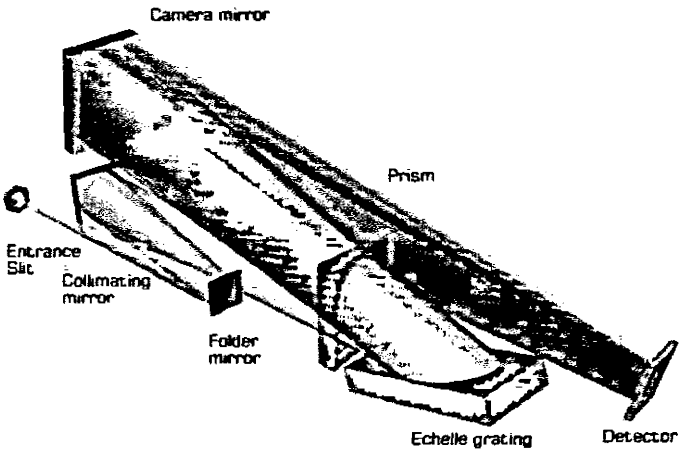

Figure 2.3 Czerny Turner HR 4000 spectrometer with important components

i) SMA Connector

Light emitted by the plasma enters the optical bench of HR 4000 spectrometer through this connector. The fiber optic cable is connected to the spectrometer through this connector.

ii) Slit

Slit is the aperture for the light to enter into spectrometer. It is a rectangular dark piece of material mounted at the backside of SMA connector. The size of the slit is of great importance as it determines how much light should enter into optical bench of HR 4000.

The optical resolution of a spectrometer depend on the size of the slit, the smaller the size higher resolution can be achieved but then small amount of light will enter into the spectrometer. The slit used in the present set up is 10 μm with 0.1 nm spectral resolution.

iii) Filter

Filters are used for restricting optical emission to pre-determined spectral regions. Before entering into the optical bench light passes through the filters. Both band-pass and long-pass filters are used to restrict the radiation to specific wavelength region.

iv) Collimating Mirror

After passing through the filter light strikes on the collimating mirror. It's a broadband mirror which collimate and reflects light towards the grating of the spectrometer.

v) Grating

Grating is the major and important part of spectrometer. The collimating mirror shines the light on the grating, which disperses the light according to their color and directed towards the focusing mirror. Gratings are available in various grooves/mm, depending on the range of the wavelength and the spectral resolution.

vi) Focusing Mirror

The reflected light from the grating falls on the focusing mirror, which focus the light onto the CCD detector or L2 detector collection lens (depending on the configuration of the spectrometer).

vii) L2 Detector Collection Lens

L2 Detector Collection Lens is another important component of this specific spectrometer. It is attached to the CCD detector. It is used to collect the light from a tall slit and focused onto the CCD detector elements.

viii) CCD Detector

The detection of light in HR2000 spectrometer is made using linear CCD arrays. The optical emissions are converted into digital signal. The CCD performs four tasks in generating an image, i.e. charge generation, charge collection, charge transfer, and finally the charge detection. In the first step, free electrons are generated due to incident photons, which are collected in the nearest collecting site, referred to as pixels. Pixels are the

electrodes, called gates formed on the surface of the CCD. The voltage on the gates is manipulated in a systematic way so that electrons move down vertically from one pixel to the next pixel. The columns act as a horizontal register of pixels, which collects a line at a time and then transfer the charge packets in serial to output amplifier by the on-chip amplifier. This voltage is amplified, processed and digitally stored in a computer to reconstruct image on the screen. CCDs provide the multichannel advantage of array detectors and since it is a two dimensional array, it can record multiple spectra simultaneously. The large format, two-dimensional nature of CCDs is ideal for high-resolution or echelle spectroscopy.

2.3 Measurement of Laser Energy

The laser is controlled very precisely by LIBS2500+ in the externally-triggered mode, but still there is a possibility that the energy may fluctuate form pulse to pulse. Therefore, for reliable LIBS measurements, the energy of the laser pulse must be measured in every shot. In the present work, the energy of the laser pulse was measured using a highly sensitive energy meter, 3-Sigma, Coherent, USA. For online energy measurement, a beam splitter of known value (90:10) is used to split the laser light into two beams. The 10 percent of the total energy is shine on the detector for the measurement the energy of the laser pulse. The remaining 90 percent of total laser energy is used to generate plasma on the surface of the target. As the breakdown threshold of material is high enough, therefore, the laser pulse is focused by a double convex lens for closed contact and beam expander assembly for standoff arrangement. The energy per unit volume increases exponentially and reaches the breakdown threshold just before the focal point.

2.4 Cross sectional area of Gaussian beam

In order to produce enough plasma on the target surface, the knowledge of energy density of a laser beam is of worth importance. Generally the laser beam has not enough energy to create plasma; therefore, it has to be focused on the target surface to achieve the threshold energy density. Since the laser used in the present experiments is of Gaussian intensity profile, therefore the energy density is determined by using diameter of Gaussian beam. The diameter of Gaussian beam is defined as radial distance between

points at which the beam irradiance has fallen to $1/e^2$ (0.135 times) of its maximum value. The radial intensity of a simple Gaussian beam is distributed in such a way that the maximum intensity is concentrated in the central part as shown in **Fig. 2.4** and mathematically expressed as:

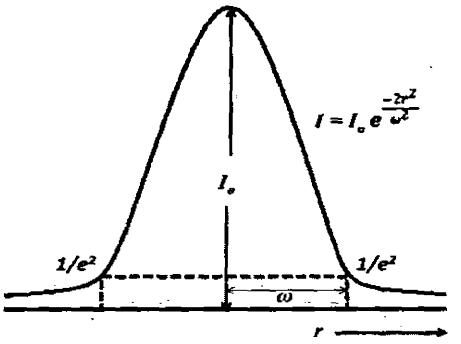

Figure: 2.4Gaussian Beam Intensity Distribution.

$$I = I_o e^{\frac{-2r^2}{\omega^2}} \tag{2.1}$$

Where I_o is the maximum intensity and ω is the beam waist (or radius). When a Gaussian beam is focused by a focusing lens of focal length f, the spot size in the beam waist (at the focus)

$$\omega_o = \frac{f\lambda}{\pi\omega_z} \tag{2.2}$$

Here $\omega_o$is half the spot size of the laser beam on the focusing lens. To reduce the diffraction losses, the diameter d of the lens should be $d \geq 3\omega_z$.The Gaussian beam is then expands and diverges from the focus point as shown in **Fig 2.4**.The diameter $\omega(z)$ of the expanded beam at any distance z from the focus point can be calculated as:

$$\omega(z) = \omega_o \sqrt{1 + \left(\frac{\lambda_l z}{\pi\omega_o^2}\right)^2} \tag{2.3}$$

$$\omega(z) = \omega_o \sqrt{1 + \frac{z^2}{z_R^2}} \tag{2.4}$$

Where, $z_R = \frac{\pi\omega_o^2}{\lambda_i}$,is known as Rayleigh range. It is also referred as the depth of the focus when focusing a Gaussian beam. At a distance $z = z_R$, $\omega(z) = \sqrt{2}\omega_o$

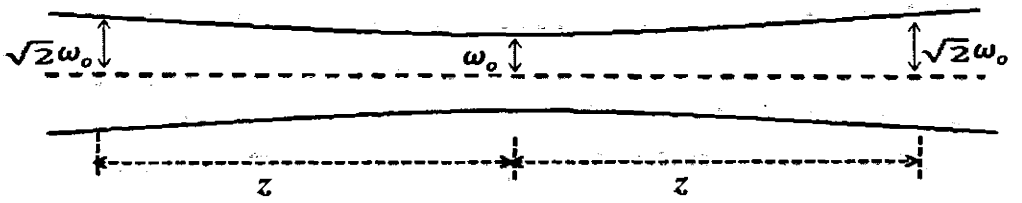

Figure: 2.5Gaussian beam parameters associated with the minimum beam waist.

Using the above parameters, the cross-sectional area of a Gaussian beam in the confocal limit can be calculated as:

$$A = \pi\omega_o^2 \left[1 + \left(\frac{\lambda_i z}{\pi\omega_o^2} \right)^2 \right] \tag{2.5}$$

2.4.1 Focusing of laser beam at large distance

2.4.1.1 Spot radius

For a given laser pulse, power density created on the surface of remote target will mainly depend on minimum spot radius w as shown in **eq. (2.1)** for a Gaussian beam is a function of distance r, the beam quality parameter M^2 ,wavelength λ and laser beam diameter at focusing optics D:

$$w = \frac{2\lambda r}{\pi D} M^2 \tag{2.6}$$

For a Gaussian beam value of $M^2 \approx 1$. Obeying the classical optics laws the diameter of the focus point linearly increase with the focusing distance due to diffraction. The nanosecond pulse has limited use in the operational range due to difficulty in tightly

focusing the beam at longer distances. Increase in distance would require extra high laser energy and large focusing optics, which will prohibit practical use of this application. At longer distances the threshold laser irradiance of 1 GW/cm^2 may become unachievable.

2.4.1.2 Depth of focus (DOF)

Another important parameter which affects laser focusing at larger distances is depth of focus of beam which is a measure of how accurately the focus must be adjusted to produce high power density on the remote target. It is defined as twice as long as the Rayleigh length, which is the distance between the two positions from the laser waist at which the area of the beam has doubled.

$$DOF = \frac{8\lambda}{\pi}\left(\frac{r}{D}\right)^2 M^2 \tag{2.7}$$

Above equation shows that the depth of focus varies as the square of distance 'r' and reciprocal of the square of input beam diameter 'D'. As a result, at longer distances DOF becomes high and hence focusing becomes less precise and accurate. Moreover, high quality anti reflection optics High anti reflection optics must be used to maximize the laser energy at the target sample.

2.5 Experimental Set up

In the present work, a series of experiments have been performed using two different kind of experimental set ups. One for closed contact experiments, in which target, laser beam delivery system, light collection system and the detection system were placed together in one place. The other experimental setup is called the standoff arrangement, in which the target is at a remote distance from all other components.

2.5.1 Closed Contact arrangement

2.5.1.1 Single Pulse LIBS

The experimental set up that was used to carry out the detection and analysis of trace elements under closed contact arrangement is shown in **Fig. 2.8**. A Q-switched Nd: YAG laser operating at 1064 nm with pulse duration of 10 ns and repetition rate of 10 Hz was used to generate plasma on the target surface. The laser beam having energy 70 to 80

mJ/P was focused onto the target surface at right angle with 20 cm focal length lens. The energy range selected for these experiments and the soft focusing on the target surface helped to avoid signal saturation. The standard samples of aluminum and low steel alloys, provided by central analytical facility PINSTECH, have been used in these experiments. These alloys were in the form circular disc. Each sample was placed on rotating stage to provide fresh surface for each laser pulse. The surface of the sample has been cleaned by firing laser shots before performing actual experiment, which made the sample a good representative of bulk sample. The emissions from the plasma were collected and directed on the entrance slit of a monochromator via multimode fiber with SMA connector. The other end of the fiber is connected to LIBS 2500+ spectrometer to transfer the emitted light to the spectrometer. The detection system comprises seven HR2000+ miniature fiber spectrometer and the linear CCD array. The overall spectral range of these spectrometers is 200-980 nm with resolution of 0.1 nm, whereas the integration time of the detector is 2.1 ms. The OOLIBS software read the data and display it in the form of a spectrum. The LIBS system triggered the Nd: YAG laser and the Nd: YAG laser and LIBS system is synchronized through lamp synchronization. Under these settings, the spectra has been recorded and analyzed through the OOLIBS software.

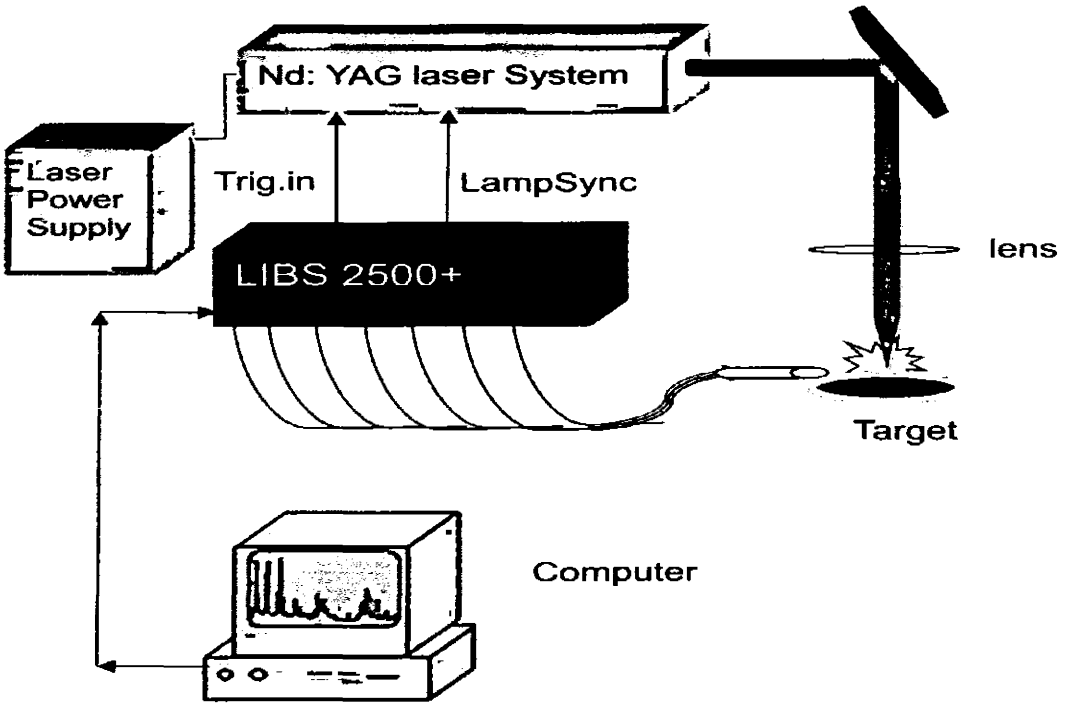

Figure 2.6 Experimental setup of LIBS in closed contact.

2.5.1.2 Double Pulse LIBS

Experiment has carried out using double pulse LIBS, in which two delayed laser pulses from two different laser systems have been used in collinear configuration. The first laser was Nd:YAG, Quanta- Ray (1064 nm, 10 Hz, 7-9ns) and the second laser was Nd:YAG, PRO-230 (1064 nm, 30Hz, 10ns). Both the lasers were synchronized and coupled using delay generators and necessary electronics as shown in **Fig 2.7**. Both the laser beams were arranged in collinear configuration with energies varied from 40 to 80 mJ respectively and the inter-pulse delay was from 0-15 μs. The energy ratio has been optimized by keeping the energy of second laser greater than first laser, whereas the inter-pulse delay has been varied using delay generators. The schematic diagram for the double pulse arrangement is shown in **Fig 2.7**.The turnip was used for the qualitative analysis of trace / heavy elements on the skin and inner of the turnip.

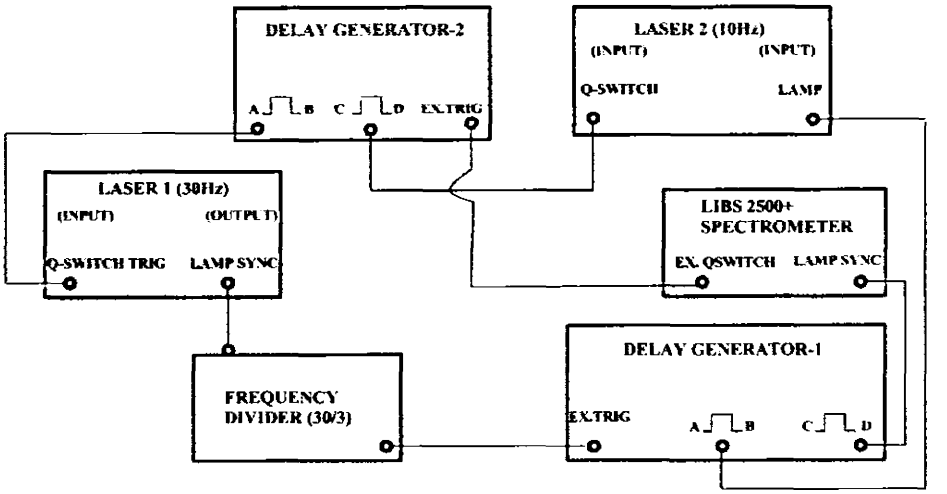

Figure 2.7 Block diagram of double pulse arrangement.

2.5.2 Standoff arrangement

In this part of the experiment, our objective was to get the emission spectra from the sample, without physically approaching the sample location. Under this arrangement, plasma is generated on the surface of a sample and the emissions are collected at a distance from the target, which is called standoff detection. In order to do the qualitative analysis of the soil sample at a standoff distance, the soil samples have been placed at the distance of 2 m and 5 m from the laser system and the light collection system. The soil has been pressed in press and shaped in the form disc of 10 mm diameter and 3mm thickness. The sample was placed on rotating stage to provide fresh surface for each laser pulse. Under this arrangement, the laser beams were expanded and then focused on the distant target via beam expander assembly. As a result of laser matter interaction, plasma is generated and the emissions are produced. The radiations are emitted in all directions and are collected through Newtonian telescope and focused on the optical fiber for onward transmission to the LIBS plus set up.

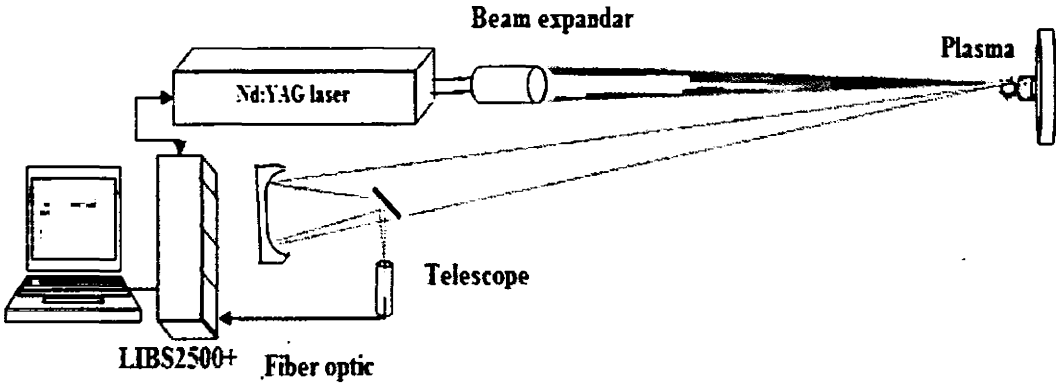

Figure 2.8 Standoff experimental set up.

2.5.3 Beam expander

When the target is at a remote distance from laser beam, the laser beam is focused using beam expander instead of single focusing lens. Beam expander is the combination of optics, which first expand the beam and then focus at the target surface. The most common type of beam expander is the Galilean telescope which usually has one concave lens as negative input lens and other is a convex lens (a positive collimating lens). As shown in **Fig.2.9** the input lens presents a virtual beam focus at the output. In order to focus the beam at a distant target, the spacing between the lenses denoted as "x" is adjusted in such a way to produce the most intense plasma at the surface of a distant target. The overall length of the optical system is given by

$$\text{Overall length} = f_1 + f_2 \tag{2.8}$$

And the magnification is given by

$$\text{Magnification} = \frac{f_2}{f_1} \tag{2.9}$$

$$p_1 = f_1 + x_1 \tag{2.10}$$

$$\frac{1}{f_2} = \frac{1}{p_1} + \frac{1}{p_2} \tag{2.11}$$

Using $p_2 = x_2$ in the above formula:

Using the following equations

$$p_1 = f_1 + x \tag{2.12}$$

Using lens formula:

$$\frac{1}{f_2} = \frac{1}{p_1} + \frac{1}{p_2} \tag{2.13}$$

Using $p_2 = d$

$$\frac{1}{f_2} = \frac{1}{f_1 + x} + \frac{1}{d} \tag{2.14}$$

$$x = \frac{df_2}{d - f_2} - (-f_1) \tag{2.15}$$

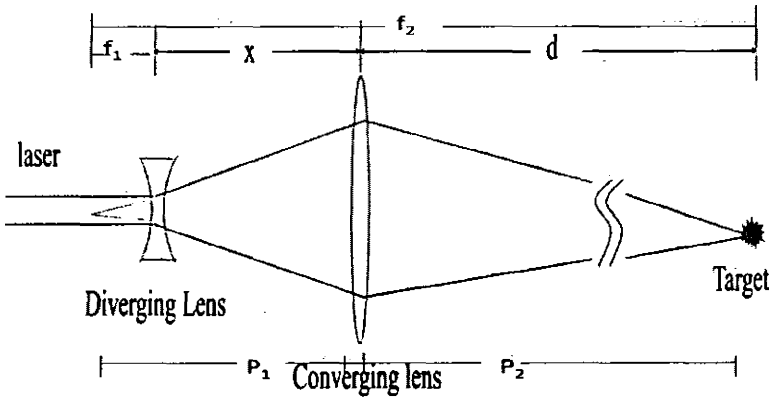

Figure 2.9 Ray diagram of beam expander.

When Galilean telescope is used to focus the laser pulses, the use of high quality anti-reflection coated optics is vital to maximize the power density transmitted to the target. The authors concluded that for stand-off LIBS analysis, it was necessary to use a good spatial laser intensity distribution and optics with minimum aberration. This is because by using two lenses for distant focusing, a decrease in the total plasma emission (represented

by number of photons emitted by the plasma per steradian) was observed as the lens to sample distance increases.

2.5.4 Newtonian Telescope

In standoff arrangements, the plasma emissions from the distant object are collected by telescope. Different receiving telescopes are used each with advantages and disadvantages. In the present work, plasma emissions were gathered by employing Newtonian telescope. This is the most simple and effective telescope configuration and can be developed using relatively less optical components. As shown in **Fig. 2.10**, the emissions are allowed to fall on the primary parabolic mirror having 10cm diameter and 100 cm focal length. This mirror brings all the points of the image into the focus at the same place. The diagonal mirror is a flat mirror, placed at the focal plane of the primary mirror, which divert the light from the path and directed on the entrance of fiber.

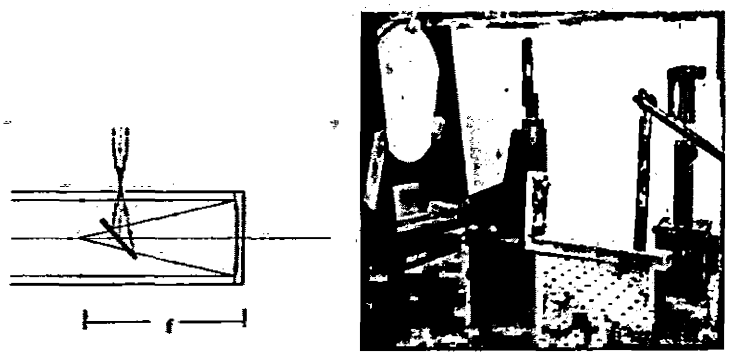

Figure 2.10 Arrangement of newtonian telescope (reflecting telescope)

Chapter No. 3

Results and discussions

Experiment No 1

3.1 Qualitative analysis of trace elements in Aluminum alloy

3.1.1 Summary

In this experiment, plasma has been produced in air at atmospheric pressure on the surface of the aluminum alloys (ALUSUSSE 412, 413) by focusing 1064 nm wavelength of Nd: YAG laser. The emission spectra from the plasma have been recorded using LIBS 2500+spectrometer, equipped with CCD detector. The emission spectra have been analyzed using the OOILIBS and Origin-8 software for qualitative analysis of the trace elements using the atomic spectra database NIST. Five trace elements have been identified from the analysis of the emission spectra and the intensities follow the relative concentration of the elements present in a sample. Chromium due to its low concentration (0.033%) present in both the alloys have been selected for the qualitative analysis in closed contact arrangement, as well as, the analysis have been performed at standoff distance of 2 and 5 m.

3.1.2 Emission spectra of Aluminum alloy

The emission spectra of the aluminum alloys were recorded using 1064 nm wavelength at 70 mJ/Plaser energy as shown in **Fig. 3.1**. The laser energy was optimized to avoid the saturation and self-absorption effects in the emission spectra. Furthermore, the optimization to record emission spectra was achieved by adjusting the Q-switch delay - 2.1 μs and gate width was fixed at 2.1 ms. The emission spectra have been analyzed using the NIST atomic spectra database [50]. In this figure, the high intensity lines are mostly Al transitions along with few Fe transitions.

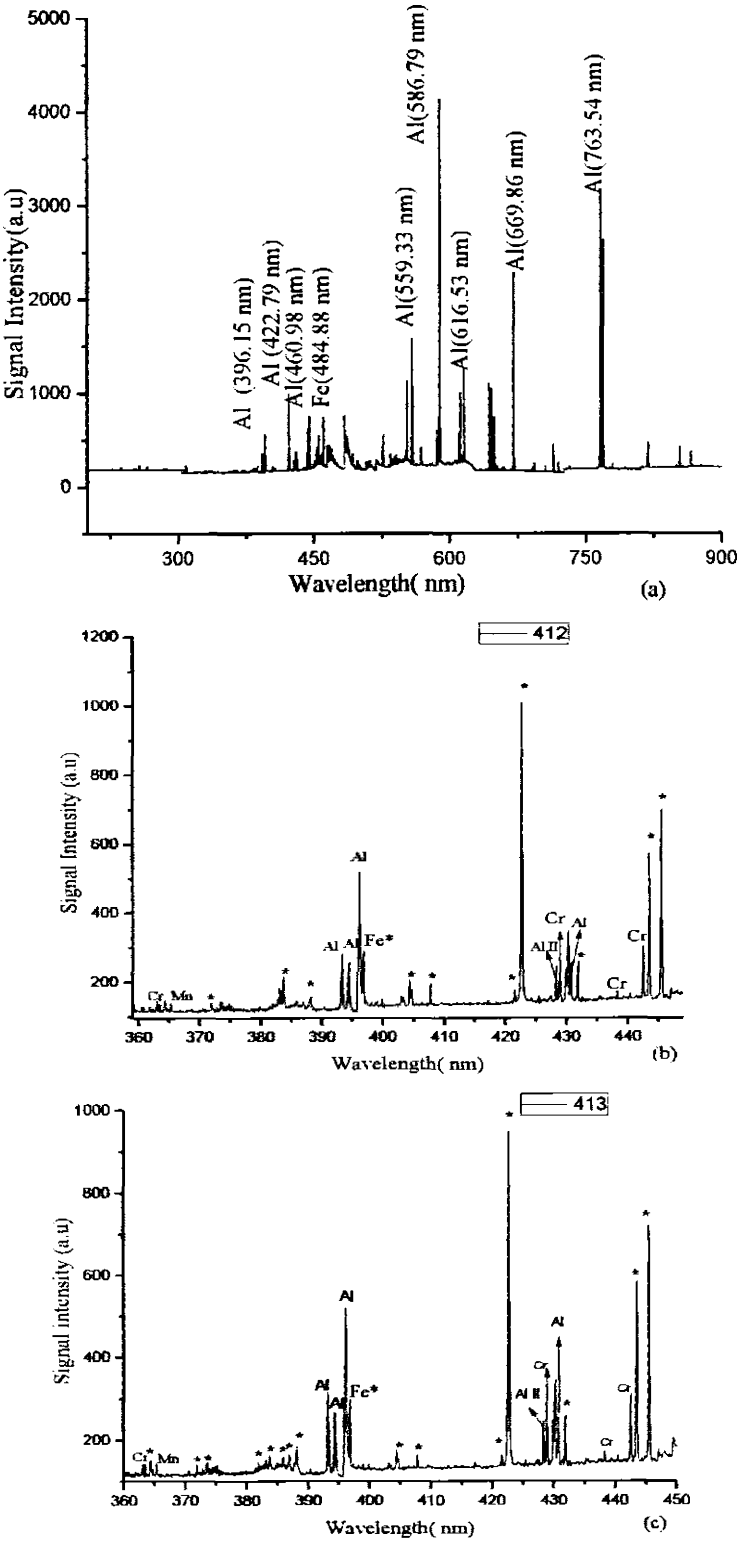

Figure 3.1 (a,b,c) Portion of emission spectra of Al-alloys (412, 413) generated using 1064 nm at laser irradiance of 70 mJ/pulse. a) emission spectrum of Al-alloy within the

wavelength range of 200-980 nm. b) emission spectra of Al 412 within wavelength range of 360-450 nm c) emission spectra of Al 412 within wavelength range of 360-450 nm

The portion of the emission spectra of aluminum alloys (412, 413) from 360 to 460 nm range has been selected in which the trace elements chromium and iron along with aluminum transitions as shown in **Fig. 3.1 (a,b,c).** The three Cr I line at 429.02, 438.19 and 442.49 nm are also identified at trace level. The assignments of the transitions have been made using L-S coupling scheme and the wavelength of the transitions have been assigned using NIST database. The emission lines from these elements, their wavelengths and transitions are listed in **Table 3.1**. Sabsabi et al. [22] analyzed the emission spectrum of aluminum alloys AL6010 and AL3003reporting the trace elements like iron, copper, magnesium, manganese and silicon. In their work, they observed that the signal intensity of trace elements is relative to their concentration in that particular sample.

Table 3.1Wavelengths, transitions and the intensities of the elements present in Al-alloy (412, 413).

Wavelength (nm)	**Transition**
Al I 393.19	$3s^3 3p(^3P^o)3d^2D^o_{5/2} \rightarrow 3s^2 4d^2D_{5/2}$
Al I 394.40	$3s^2 4s\ ^2S_{1/2} \rightarrow 3s^2 3p^2S_{1/2}$
Al I 396.15	$3s^2 4s\ ^2S_{1/2} \rightarrow 3s^2 3p^2P^o_{3/2}$
Al II 428.29	$3s11f\ ^1F_3 \rightarrow 3s4d^1D_2$
Al I 430.72	$3s12p\ ^1P^o_{1/2} \rightarrow 3s4d^1D_2$
Fe I 396.79	$3d^6(^5D)4s(^6D)4d^7G_4 \rightarrow 3d^6(^5D)4s4p(^3P^o)^5D^o_3$
Al II 422.68	$3s8f^3F^o_4 \rightarrow 3s4d^3D_2$
Fe I 430.21	$3d^6(^3F_2)4s4p(^3P^o)^3G^o_4 \rightarrow 3d^7(^2G)4s^1G_4$
Fe I 443.51	$3d^6(^5D)4s4p(^3P^o)^7F^o_1 \rightarrow 3d^64s^{25}D_2$
Fe I 445.43	$3d^6(^3P_2)4s4p(^3P^o)^3D^o_2 \rightarrow 3d^7(^4P)4s^3P_2,$
Cr I 438.11	$3d^4(a^3P)4s4p(^3P^o)^5P^o_1 \rightarrow 3d^5(^4P)4s^5P_2$
Cr I 442.42	$3d^5(^4P)4p^5P^o_3 \rightarrow 3d^5(^4D)4s^5D_4$
Fe I 360.48	$3d^6(^5D)4s(^6D)4d^5D_o \rightarrow 3d^6(^5D)4s4p(^3P^o)^7F^o_1$
Fe I 361.31	$3d^6(^5D)4s(^6D)4d^7P_2 \rightarrow 3d^6(^5D)4s4p(^3P^o)^7F^o_2$

Fe I 361.83	$3d^7(^4F)4d^5G_4 \rightarrow 3d^6(^5D)4s4p(^3P^o)^5D^o_3$
Fe I 362.35	$3d^6(^3G)4s4p(^3P^o)^5H^o_5 \rightarrow 3d^64s^{23}F^2_4$
Fe I 363.03	$3d^6(^5D)4s(^6D)4d^5D_3 \rightarrow 3d^6(^5D)4s4p(^3P^o)^7F^o_4$
Fe I 364.35	$3d^6(^3G)4s4p(^3P^o)^5H^o_3 \rightarrow 3d^64s^{23}F_2$
Cr I 363.52	$3d^4(^5D)4s4p(^3P^o)^7D^o_3 \rightarrow 3d^5(^6S)4s^7S_3$
Mn I 360.79	$3d^6(^5D)4p^6P^o_{7/2} \rightarrow 3d^6(^5D)4s^6D_{7/2}$
Mn I 364.69	$3d^6(^5D)4p^4F^o_{5/2} \rightarrow 3d^6(^5D)4s^6D_{7/2}$
Mn I 365.29	$3d^6(^3G)4p^5F^o_{5/2} \rightarrow 3d^6(^3F2)4s^4F_{5/2}$

3.1.3 Trace detection of Cr and Mn at closed contact at standoff distance

The portion of the emission in the range from 361-368 nm is shown in **Fig 3.2**. It represents the spectrum of standard aluminum sample (ALUSUSSE412). The most persistent lines in Al-alloys are Cr at 363.52 nm with lowest concentration.

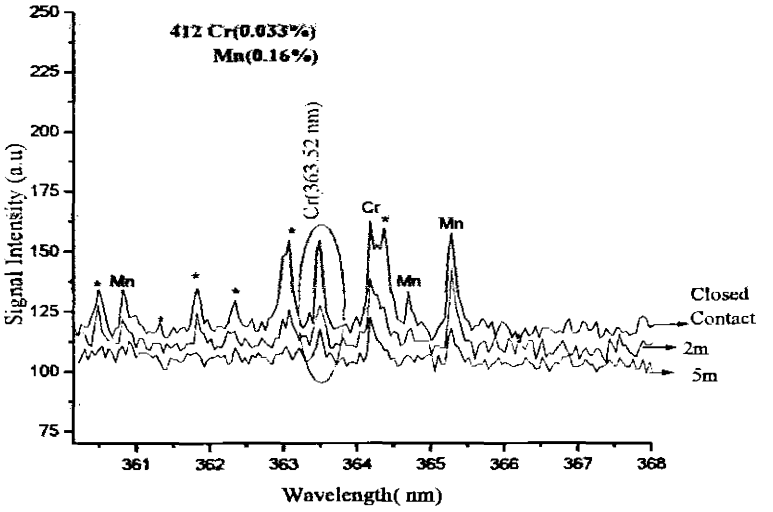

Figure 3.2 Spectrum of Al-alloy 412Cr I 363.52 nm within wavelength range of 356 nm to 368 nm in closed contact 2m and 5m

Therefore, the emission spectrum of Al 412 in the 360 up to 368 nm in closed contact and at distances of 2m and 5m.The trace elements Cr and Mn has been selected for comparison. As the Cr has lowest concentration of 0.033% and of Mn is 0.16%.in the sample 412. The top trace is the emission spectra recorded in closed contact arrangement, whereas the middle and the lower traces are the spectra at a standoff distance of 2 and 5

meter. Thus, if we increase the distance of the sample from laser, the observed intensity is decreased to $(1/2)^2 = 1/4$ of its original value. The comparison of intensities of trace elements indicates decreasing trend with the increasing distance as mentioned by $I = \left(\frac{1}{d}\right)^2$. The spectrum shown in **Fig. 3.2,** demonstrate that the spectrum has been normalized first. Therefore the signal intensity can be compared to each other in closed contact as well as at a standoff distance. The signal intensity of Cr (363.52 nm) line is higher in Al-412 as compared to Al-413. This intensity variation is in accordance with the concentration of Cr in both alloys.

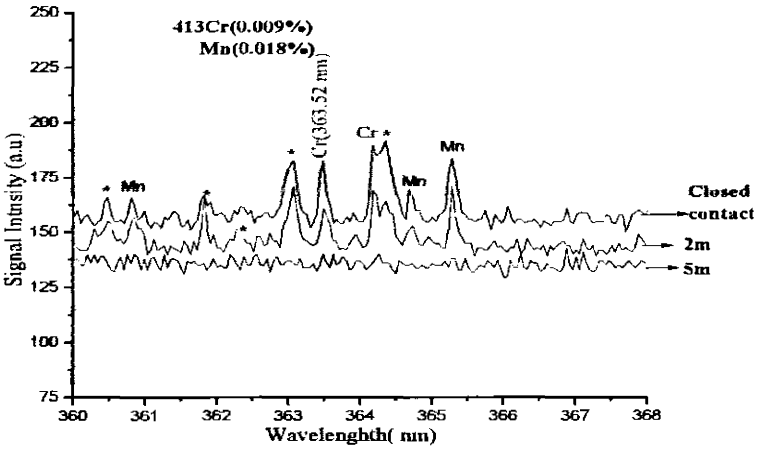

Figure 3.3Spectrum showing comparison of signal heights of Cr I 363.52 nm within wavelength range of 356 nm to 368 nm in closed contact,2m and 5m in Al-alloy413.

The ability of LIBS to detect trace impurities in aluminum alloys is shown in **Fig 3.3.** The region selected in this figure comprises Cr, Mn, and Fe as a trace element, among which chromium is present with 0.0035% concentration and Mn is 0.018%.Intensity is power divided by the area over which that power is spread. For lasers, the power is spread out over the surface of a circular spot. As the beam propagates, the radius of this spot (called **w**) increases linearly. The area of this spot is $\pi\omega^2$. Since ω is proportional to r, the area of the spot is also proportional to r^2, just like for the point source. To compare the results, all the three sets of spectra have been captured at the same 70 mJ per pulse. The inspection of **Fig 3.3** shows the capability or sensitivity of the LIBS system for qualitative analysis of trace elements in (alloy) 413.The trace elements lines are observed at a standoff distance of 2m and 5m.It is evident from **Fig. 3.1 (b,c)** that there is

a clear difference in intensities of trace elements and the parent element, except the iron lines which being a trace element have more intensity. As chromium is present in trace amount so its intensity as expected is much lower than the aluminum. Because the emission intensity is proportional to the concentration of that element in a sample as explained:

$$I = \frac{1}{4\pi} A_{ip} h\nu_{ip} N_o \frac{g_u e^{-E_u/KT}}{Z(J)} \tag{3.1}$$

According to **eq. (3.1),** one can determine the population density of the relevant species (atoms or ions) for an element in plasma from a measurement of the absolute intensity of corresponding transition and knowledge of the excitation temperature and atomic constants. However, it is not possible to derive a theoretical expression relating N and concentration of that element in solid sample under investigation. Hence, in practice, an empirical relation is sought between the observed line intensity (I) and corresponding concentration (C) i.e.

$$I = F(C) \tag{3.2}$$

Here F (C) is called analyte calibration function and the graph between the LIBS intensity of a line of specific element and the concentration is called calibration curve. Such curve can be drawn by measurement of reference samples of known concentrations termed as standard samples and can be used to determine the elemental concentration in unknown sample.

Table 3.2 Composition and percentage concentration of Al-alloys.

Alloy-samples	*Cr (%)*	*Mn(%)*	*Fe (%)*
ALUSUSSE 412	*0.033*	*0.16*	*0.36*
ALUSUSSE413	*0.0035*	*0.018*	*0.13*

The second lowest concentration element in Al-412 and Al-413 alloys is Mn, the qualitative analysis of Mn I (365.23 nm) line. This is a non-resonance transition with transition probability 7.4e+06 s^{-1}. The inspection of **Fig 3.3** shows that this line has sufficiently high intensity in closed contact, which systematically decreases with distance

from the target surface. Sabsabi et al. [22] recorded the emission spectra of aluminum alloy samples AL6010 and AL3003 for quantitative analysis. Their emission spectra can be compared to our work. As in, the emission spectra have strong magnesium lines and weak silicon lines. But there is absence of chromium in the spectra although it is constituent of the samples. In the same way, in **Fig. 3.2 and 3.3** lines of chromium, manganese and iron are present but there is absence of magnesium lines whereas it is also present in trace amount in Al-alloys.

3.1.4 Comparison of signal intensity of chromium in two samples having different concentration of Cr

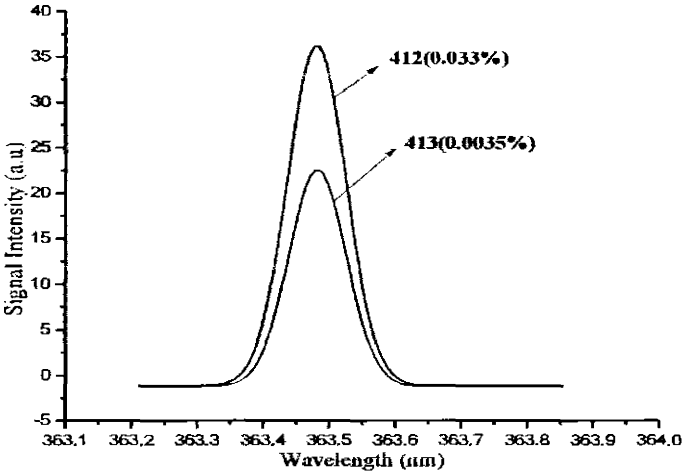

Figure 3.4 Difference in signal intensity of Cr(363.52 nm) relative to concentration in three samples412 (0.033%), 413 (0.0035%).

Fig. 3.4 illustrates the line profile of Cr (363.52 nm) in closed contact arrangement. Three Al-alloys having different concentrations of Cr has been selected. These are the 0.0035% and 0.033%. In order to obtain a fair comparison of the line profile between the signal height and relative concentrations, one must record the emission spectra of all three samples under the same experimental conditions and study their relative intensities with respect to their concentration.

Experiment No. 2

3.2 Qualitative analysis of trace elements in steel alloy

3.2.1 Summary

The emission spectra of steel alloys (AISI 401, 405) have been recorded with the fundamental harmonics (1064 nm) of Nd: YAG laser using LIBS2500+ spectrometer. The qualitative analysis of the emission spectra consists of strong Fe lines, whereas, sulphur, iron, chromium, molybdenum and nickel was observed as trace elements in which the molybdenum has lowest concentration (0.002%). In addition, the trace level detection has been carried out at a standoff distance of 2m and 5m.

3.2.2 Emission spectra of steel alloys

The emission spectra of steel alloys AISI 401 have been recorded using in the 200-980 nm range as shown in **Fig. 3.5**. The emission spectra have been optimized to reduce the effects of continuum radiations to avoid the saturation and self-absorption effects. As the steel alloy has rich spectra of strong and intense Fe lines, therefore of the spectra the energy was optimized to 80 mJ/pulse. In these experiments, plasma has been generated on the surface of steel alloy. Therefore to compare the results, the normalization of the spectra has been made by adjusting the sample and lens distance.

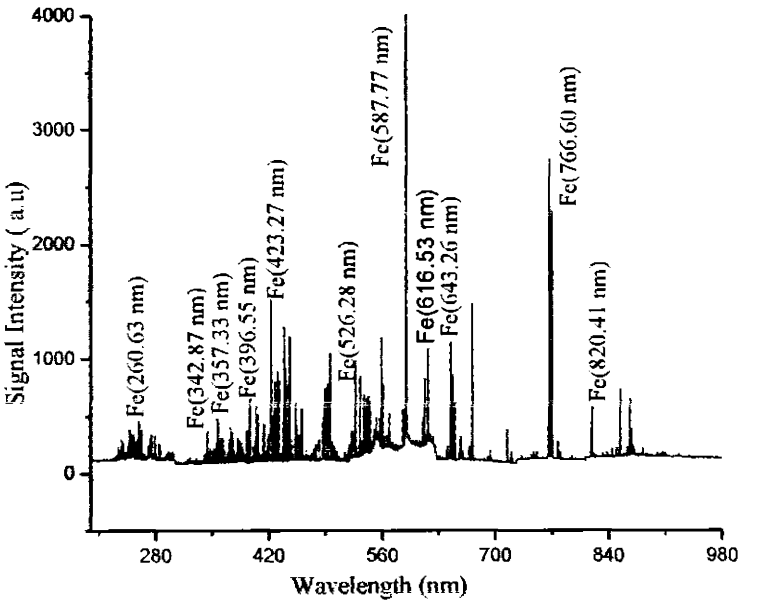

Figure 3.5 Typical emission spectrum of steel alloy AISI (401) within the range of 200 - 980 nm.

3.2.3 Trace detection of S and Mo in closed contact and at standoff distance of 401 steel alloy

The portion of the emission spectra of steel alloy (401) from 530 to 580 nm range has been selected in which the trace elements sulphur and molybdenum along with iron transitions as shown in **Fig. 3.6.**This specific region comprises of emission lines of trace elements sulphur, nickel, chromium, molybdenum and iron. According to the data provided with this sample, sulphur is present in the lowest quantity, whereas iron has highest transition probability that is the reason for the presence of strong iron lines.

Table 3.3 Composition of reference samples of steel alloys.

Steel-alloys	*S (%)*	*Si(%)*	*Mn(%)*	*Mo(%)*	*Ni(%)*	*C(%)*
AISI 401	*0.009*	*0.41*	*0.85*	*0.47*	*0.031*	*1.06*
AISI 405	*0.069*	*1.71*	*1.28*	*0.002*	*0.22*	*0.032*

The trace element sulphur also follow the intensity selection rules as evident from the multiplet structure around 571 nm, which confirmed that the spectra has been recorded under well controlled environment as no self-absorption can be seen in this spectrum.

In **Fig 3.6,** Spectrum of steel alloy 401 recorded in closed contact has been shown. The spectral lines used for the analysis were Fe I lines .Fe I is the main constituent of steel sample, therefore Fe I has strong emission line 568.65 nm in this region together with the weak iron line 568.15 nm. The difference in signal intensities follow the intensity pattern given in NIST database may be due to different values of transition probabilities of these lines. Detection of trace-level concentrations in steel alloys using LIBs has been investigated in open air. This spectral region revealed the presence of five trace elements including sulphur, molybdenum, silicon, chromium and nickel. The trace element sulphur also follows the intensity selection rules as evident from the multiplet structure around 571 nm.

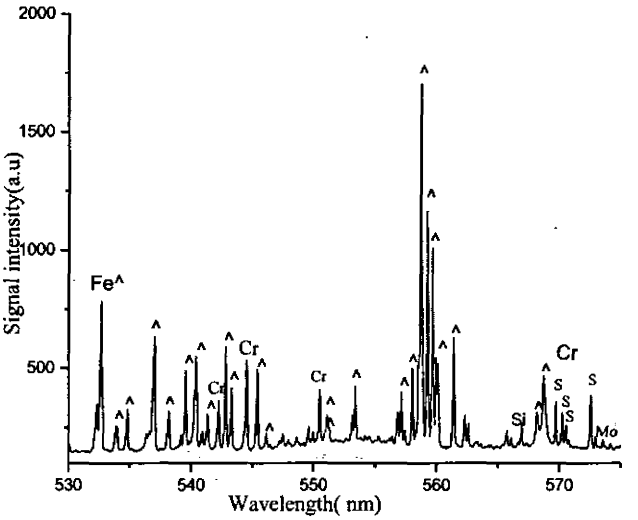

Figure 3.6 Spectrum shows the emission lines of iron as well as trace elements sulphur, nickel, chromium and molybdenum.

Guo QJ et al. [56] presented their work on a series of steel alloys GBW01605-01609 samples. The experimental conditions were optimized for the applications of LIBS to the trace analysis in steel alloys were obtained firstly. They have recorded the emission spectra of steel samples and detected the minor elements present in that particular sample. In **Fig 3.7** Iron being the main constituent have intense emission lines. On the other hand, the minor elements like nickel, chromium and molybdenum also present in this spectral range but with very less signal intensity.

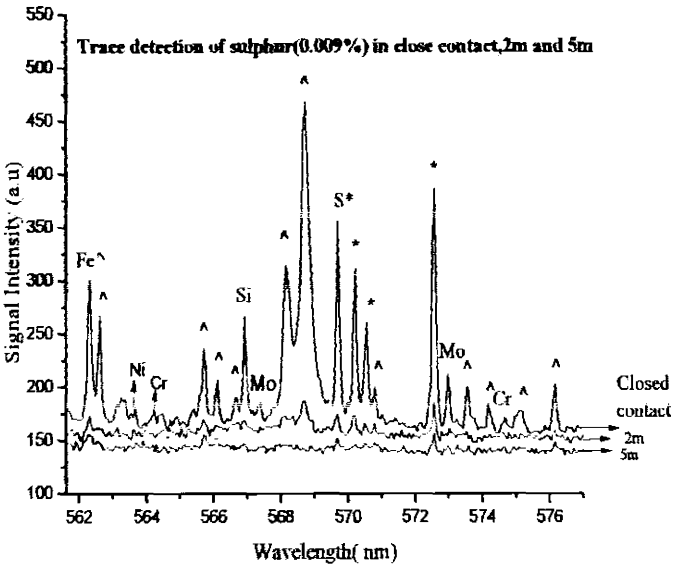

Figure 3.7Emission spectra recorded in closed contact and at standoff distance of 2m and 5m of sample AISI 401.

The comparison of emission spectra of 401 alloyin closed contact and at standoff distance of 2m and 5m is demonstrated in **Fig. 3.7**. The transitions of minor elements like nickel, chromium, sulphur and molybdenum along with major element iron are shown in **Table 3.4.**

Table 3.4 Transitions of trace elements in steel sample 401 in within wavelength range of 561 nm to 575 nm.

Wavelength(nm)	Transitions
Fe I 562.29	$3d^7(^4P)4p\ ^3D^o_2 \rightarrow 3d^64s^{23}D_2$
Fe I 562.45	$3d^6(^5D)4s(^6D)5s\ ^5D_2 \rightarrow 3d^6(^5D)4s4p(^3P^o)\ ^5F^o_2$
Fe I 565.64	$3d^64s^{23}P^2_2 \rightarrow 3d^64s^{25}D_2$
Fe I 566.13	$3d^6(^5D)4s(^4D)5s\ ^5D_1 \rightarrow 3d^6(^5D)4s4p(3P^o)\ ^3P^o_o$
Fe I 566.71	$3d^64s(^4D)4d\ ^5P_3 \rightarrow 3d^6(^5D)4s4p(^1P^o)\ ^5F^o_3$
Fe I 568.02	$3d^7(^2D_2)4p\ ^3F^o_3 \rightarrow 3d^{83}F_2$
Fe I 568.65	$3d^7(^4F)4d\ ^3H_5 \rightarrow 3d^7(^4F)4p^3F^o_4$
Fe I 570.77	$3d^6(^5D)4s(^6D)4d\ ^7P_3 \rightarrow 3d^7(^4F)4p\ ^5D^o_4$
Fe I 573.45	$3d^64s(^6D)5d\ ^5P_2 \rightarrow 3d^6(^5D)4s4p(^1P^o)\ ^5D^o_3$

Fe I 574.18	$3d^6(^5D)4s(^4D)5s\ ^3D_2 \rightarrow 3d^7(^4F)4p\ ^5F^o_3$
Fe I 574.74	$3d^7(^4F)4d\ ^5G_3 \rightarrow 3d^6(^5D)4s4p(^1P^o)\ ^5P^o_3$
Fe I 576.13	$3d^6(^3P_2)4s4p(^3P^o)\ ^3P^o_o \rightarrow 3d^64s^{23}D_1$
S I 569.66	$3s^23p^3(^4S^o)7d\ ^5D^o_2 \rightarrow 3s^23p^3(^4S^o)4p\ ^5P_1$
S I 570.02	$3s^23p^3(^4S^o)7d\ ^5D^o_3 \rightarrow 3s^23p^3(^4S^o)4p\ ^5P_2$
S I 570.61	$3s^23p^3(^4S^o)7d\ ^5D^o_4 \rightarrow 3s^23p^3(^4S^o)4p\ ^5P_3$
S I 572.58	$3s^23p^3(^4S^o)10d\ ^3D^o_2 \rightarrow 3s^23p^3(^4S^o)4p\ ^3P_2$
Cr I 564.23	$3d^44s5s\ ^5D_4 \rightarrow 3d^4(^5D)4s4p(^3P^o)\ ^5F^o_4$
Ni 563.67	$3d^9(^2D_{3/2})4d\ ^2[3/2]_1 \rightarrow 3d^9(^2D)4p\ ^1P^o_1$
Si 566.95	$3s3p(^3P^o)4p\ ^4D_{7/2} \rightarrow 3s3p(^3P^o)3d\ ^4F^o_{9/2}$

3.2.4 Trace detection of S and Mo in closed contact and at standoff distance of AISI 405

The portion of the emission spectra from 230 - 300 nm is shown in **Fig. 3.8**, Using the laser energy 80 mJ/P. The emission spectrum consists of strong Fe lines, these lines are analysis identified using NIST atomic database.

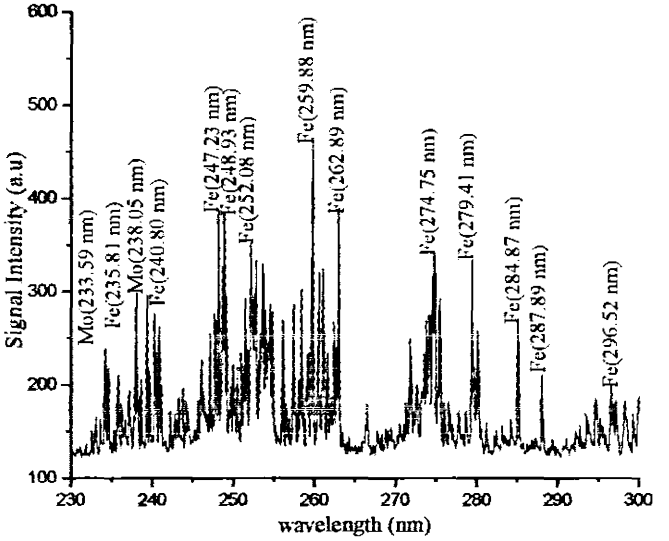

Figure 3.8 Spectrum of steel 405 alloy in closed contact within the wavelength range of 230- 300 nm.

In closed contact emission intensities are maximum because of better coupling of energy to the target sample, given away the fact that detector is placed near to the target surface and plasma has been recorded very closely as evident from **Fig 3.8.** In **Fig 3.9**, the comparison of closed contact, 2m and 5m of steel 405 samples has been demonstrated. It is clear from the figure that closed contact has highest intensity; this is because the LIBS signal must be proportional to the solid angle of collection, which is inversely proportional to square of the analysis distance. Salle et al. [1] has elaborated the parameters which affect the signal intensity at standoff distance. According to which, if we suppose that plasma conditions are not varied with the working distance, LIBS signal which is 16,000 counts at 1m would be 4000 counts at 2m and at 5m counts will be 640.

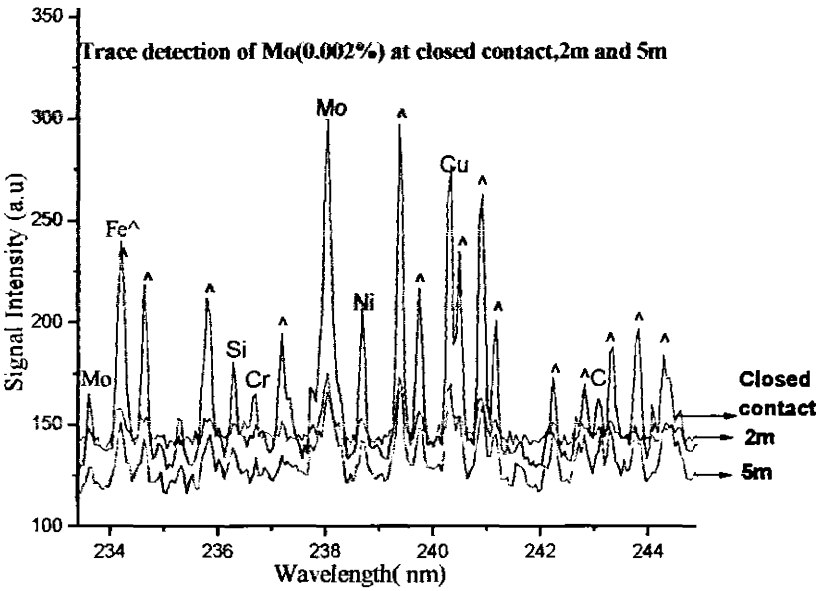

Figure 3.9 Spectrum recorded in closed contact and at standoff distance of 2m and 5m.

For obtaining better signals even at standoff distances the anti-reflection high quality optics must be employed in the setup. By using this high quality optics the laser energy on the target would be maximized, which can be reduced through process of scattering and absorption by the atmosphere and air breakdown also plays important role in reduction of intensity of laser beam.

Table 3.5 Transitions within the wavelength range of 234 nm to 245 nm in the steel alloy 405

Wavelength (nm)	Transitions
Fe I 234.25	$3d^7(^2G)4p\ ^3H^o_5 \rightarrow 3d^7(^4F)4s\ ^5F_5$
Fe I 234.63	$3d^6(^3H)4s4p(^3P^o)\ ^5G^o_4 \rightarrow 3d^64s^{25}D_3$
Fe I 235.89	$3d^6(^1G_2)4p\ ^2G_{7/2} \rightarrow 3d^6(^3G)4s\ ^2G_{7/2}$
Fe I 237.23	$3d^6(^3F_2)4p\ ^4D^o_{7/2} \rightarrow 3p^63d^{72}H_{9/2}$
Fe I 239.40	$3d^6(^5D)4d\ ^6D_{9/2} \rightarrow 3d^6(^5D)4p\ ^6F^o_{11/2}$
Fe I 239.67	$3d^6(^3G)4p\ ^2H^o_{11/2} \rightarrow 3d^6(^3G)4s\ ^4G_{9/2}$
Fe I 240.48	$3d^6(^5D)4p\ ^6F^o_{7/2} \rightarrow 3d^6(^5D)4s\ ^6D_{5/2}$
Fe I 240.80	$3d^7(^2G)4p\ ^3F^o_3 \rightarrow 3d^7(^4F)4s\ ^5F_3$
Fe I 241.19	$3d^7(^2G)4p\ ^3F^o_2 \rightarrow 3d^7(^4F)4s\ ^5F_2$
Fe I 242.31	$3d^6(^3F_2)4s4p(^3P^o)\ ^3D^o_2 \rightarrow 3d^7(^4F)4s\ ^5F_2$
Fe I 243.38	$3d^7(^4F)5p^5F^o_2 \rightarrow 3d^7(^4F)4s\ ^3F_2$
Fe I 243.81	$3d^6(^3G)\ 4s4p(^3P^o)\ ^5F^o_4 \rightarrow 3d^7(^4F)4s\ ^5F_5$
Fe I 244.26	$3d^6(^3G)4s4p(^3P^o)\ ^5H^o_6 \rightarrow 3d^7(^4F)4s\ ^5F_5$
Cr I 236.71	$3d^5(^6S)5p\ ^7P^o_2 \rightarrow 3d^5(^6S)4s\ ^7S_3$
Ni 238.77	$3p^63d^8(^3F)4p\ ^4F^o_{7/2} \rightarrow 3p^63d^8(^3F)4s\ ^2F_{7/2}$

Experiment No. 3

3.3 Qualitative analysis of trace elements in turnip using single and double pulse

3.3.1 Summary

In this experiment, we report the investigations of plasma induced by laser ablation on the surface and flesh of turnip (*Brassica rapa*). Nd: YAG laser (1064 nm) having 130mJ/pulse was used to generate plasma. The emission spectra was captured and analyzed via LIBS2500+ spectrometer and OOLIBS software. The qualitative analysis of the emission spectra reveals the presence of metals such as Fe, Ca, Hg, Zn and Cr. In addition electron density and temperature were determined using Stark broadened line profile and Boltzmann plot method. Furthermore the spatial evolutions of these metals in plasma were studied for single and dual pulse. Signal intensities follow the increasing trend in signal intensities of heavy elements when moving from center to skin of turnip, whereas in up to down profile the trend is not as regular. In dual pulse spectra signal enhancement occur with great magnitude.

3.3.2 Emission spectra of turnip skin

As turnip is a root vegetable and is in direct contact with the soil, therefore the heavy elements from the soil may absorb into the skin. Among these elements, the hazardous metal may transmit into human body causing severe damage.

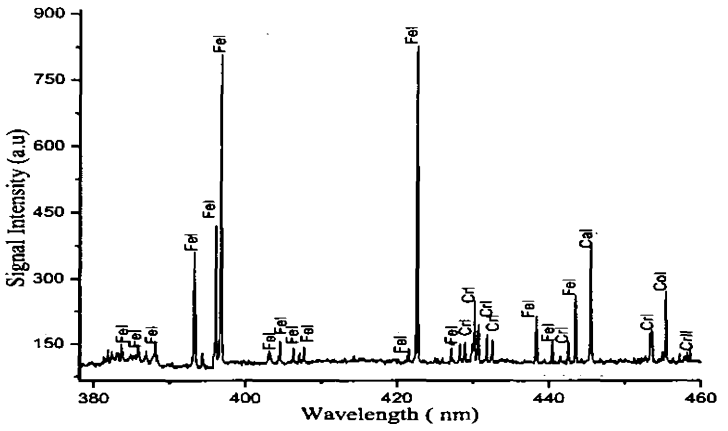

Figure 3.10 Emission spectra of turnip skin.

Fig 3.10 shows LIBS emission spectra of plasma generated on the skin of the turnip. The spectrum is in the range of 380-400 nm. This spectrum shows the emission line from the major element Ca as well as trace elements like Fe, Cr and Co. The above figure shows rich Fe spectrum.

3.4 Single pulse

3.4.1 Space resolved analysis of turnip from center to Skin for

The result of space-resolved analysis is shown in **Fig 3.11**. This shows typical distribution of these elements plotted on relative intensity basis. Few elements like Cr, Ca, Zn, Fe and Hg have been selected and the emission lines are selected under the criteria that these lines are not self-absorbed and present in each spectrum.

Table 3.6 Wavelengths and transitions of elements used for qualitative analysis of turnip

Element	Wavelength λ(nm)	Transitions
Fe	247.69 nm	$3d^7(^4P)4p\ ^3P^o_1 \rightarrow 3d^7(^4F)4s\ ^5F_1$
Cr	455.39 nm	$3d^5(^2D)4p\ ^3F^o_2 \rightarrow 3d^5(^2F_1)4s^3F_2$
Ca	866.22 nm	$3p^64p\ ^2P^o_{1/2} \rightarrow 3p^63d\ ^2D_{3/2}$
Zn	589.41 nm	Nil
Hg	871.43 nm	$5d^{10}6s10f\ ^1F^o_3 \rightarrow 5d^{10}6s6d\ ^1D_2$

It is observed from the figure that the signal intensity (alternatively the concentration of the elements) increases as we approaches towards the skin. Starting from lowest concentration elements like iron and chromium, their concentration is low in the center and increases from center to skin. Due to the direct contact with the soil these metals seep into the turnip skin. Other elements like Ca, Hg, and Zn have high relative intensities, have same increasing trend from center to skin.

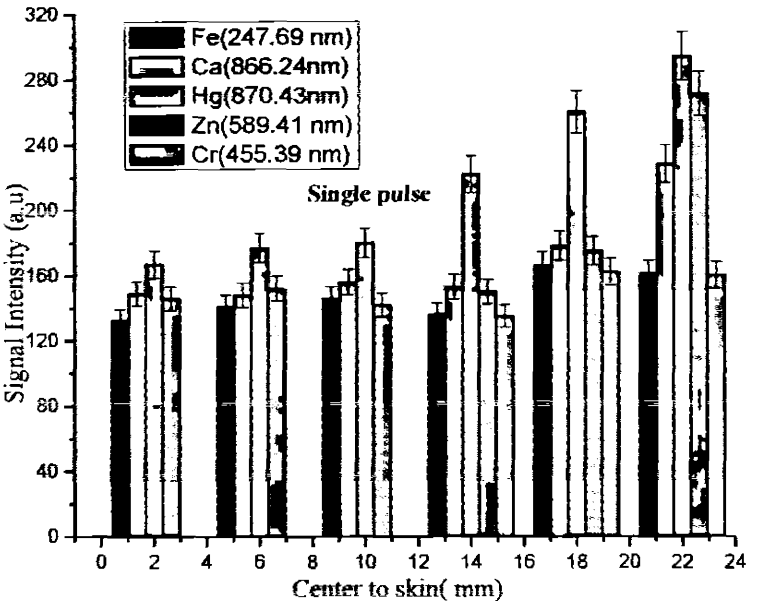

Figure 3.11 Spectrum comparing the composition of the major and minor elements and their distribution from center to skin.

Furthermore, the concentration of chromium is sufficiently high at the skin but drastically reduces inside the turnip and vanishes at half way from the center. It can be assumed from the figure that skin provides shield against the transmission of the heavy metals from soil to inside the turnip. Juve et al.[43] reported the higher concentration of Al, Ca, Ti, Mn, and Fe on the surface of the potato. But this concentration gradually decreases from skin to center. This behavior is in close agreement with our observation for turnip. In their work they reported that Mg has same concentration throughout both in potato and carrot indicating their strong penetrating power.

Unlike potato, turnip is partially inside soil and partially above the ground. In this regard the elemental distribution and their relative concentration from top to bottom is important to know.

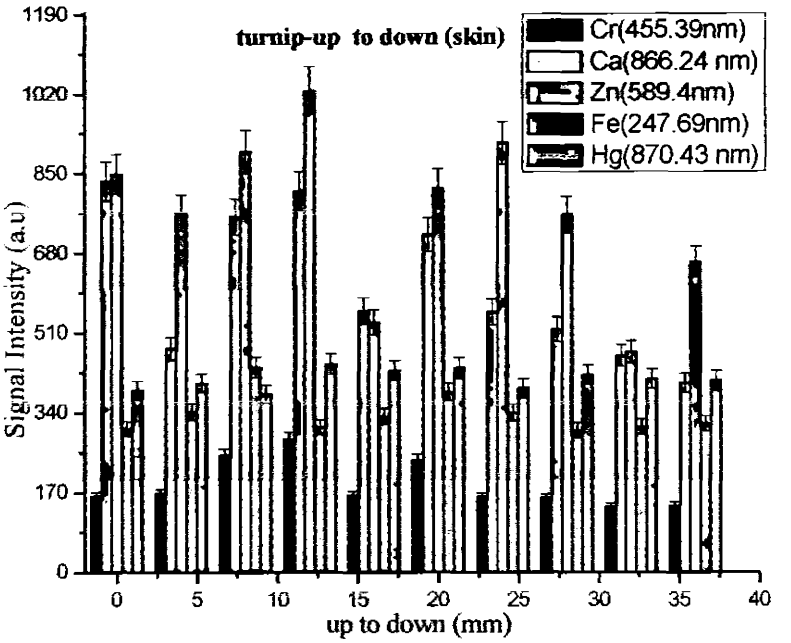

Figure 3.12 Single pulse up to down variations in emission intensities at skin.

Spectrum in **Fig 3.12** shows the variation in signal intensity of constituent elements as well as hazardous elements on different parts of the skin of turnip. The signal intensities of Cr, Ca, Zn, Fe and Hg are plotted as a function of distance from top to bottom on the skin of turnip. It is observed that the signal intensities of Ca and Zn decrease from top to bottom, it means Ca and Zn may have high concentration on the surface of the soil as compared to inside the soil. Therefore these elements have high concentration in the upper portion of the turnip compared to the portion which is under the soil.

On the other hand the elements like Hg, Fe have same concentration throughout from top to bottom. Cr is present as a trace as indicated by the relatively weak signal intensity according to **eq. (3.1).**

The concentration of the Cr is low at the upper part of the turnip, gradually increases around the portion where the turnip touches the soil. And again decrease its concentration in the portion which is inside the soil. This behavior shows that Cr is present on the surface of the soil and their seepage into the soil is very small. Further, the Cr may come from the industrial waste water or from any other such polluted and contaminated sources, mixed with water used for irrigation and from their transmission into vegetables

like turnip. It is also observed from **Fig 3.11** that half the way from skin to center the Cr vanishes whereas, it has diffusion pathway on the skin.

3.4.2 Measurement of Plasma parameters (T_e and N_e)

For characterization of plasma, the excitation temperature of an element is retrieved from Boltzmann plot method. Assumption can be made that LTE has been established within plasma. These parameters have been extracted under the LTE. This is a reliable method for electron temperature measurement.

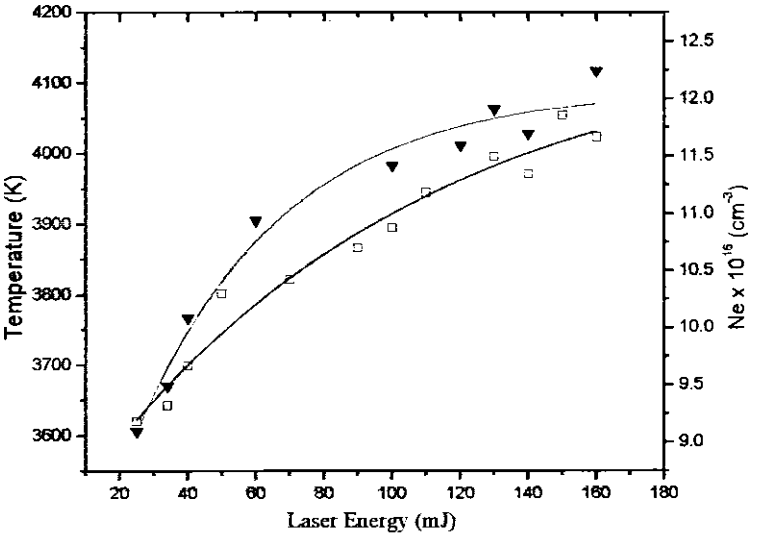

Figure 3.13 Temperature T_e and electron density N_e calculated at single pulse.

In order to measure the electron temperature of plasma, the Boltzmann plot method has been used having the following relation

$$\ln\left(\frac{\lambda_{ji} I_{ji}}{hcA_{ji} g_j}\right) = \ln\left(\frac{N}{Q(T)}\right) - \left(\frac{E_j}{kT}\right) \tag{3.6}$$

Where λ is wavelength of a given transition, A_{ji} and g_j are transition probability and statiscal weight of the upper level respectively, E_j is energy of upper level, Q(T) is partition function and N is population of upper energy level. Whereas, the electron number density has been extracted from the stark broadened line profile of Fe I (247.69.nm).Using these methods, the e-s temperature and number density has been measured and plotted as a function of laser energy as shown in **Fig 3.13**.The plasma parameters need to be measured to know about the Local thermodynamic equilibrium

(LTE). This gives the confidence that the plasma can be used for any kind of elemental analysis. The measurement of electron number density confirm the validity of local thermodynamic equilibrium (LTE) using the relation;

$$N_e \geq 1.6\times10^{12}T^{1/2}(\Delta E)^3 cm^{-3} \quad (3.7)$$

Where, *(ΔE)* is the energy difference of two levels and *T (K)* is the electron temperature. This gives the confidence that the plasma can be used for any kind of elemental analysis.

In our experiment concerning the characterization of plasma induced on turnip, iron appears to be the most appropriate element for retrieving the plasma temperature. As iron appears to be present in trace quantity but emission spectra comprises of most of the iron lines, and emission lines of iron are very consistent. Lei et al. [58] used Calines for the excitation temperature and electron number density, because these lines were comparatively stronger than other lines present in fresh potato.

For the present measurement, although the Ca emission lines are strong but we have selected Fe lines because i) Fe is present as a trace element in turnip and ii) It has lot of emission lines in the spectra as compared to other trace or major elements present in turnip. Therefore, the Fe lines have been used for the estimation of electron temperature and number density.

Double pulse LIBS of Turnip

The Double pulse LIBS technique as introduced by Cremers et al. [52] issued in the present work. In this technique two delayed laser pulses of the same 1064 nm laser wavelengths is used to generate and reheat the plasma. As this technique is used to enhance the selectivity and sensitivity of emission lines. Rizwan et al. [54] used A*l* and Mg lines and reported the maximum enhancement in signal intensity at 25 μs inter pulse delay. The two laser pulses from two different synchronized lasers have been shine on the target surface under collinear beam geometry. Gautier et al. [44] used collinear beam geometry and observe the effects of double pulse on the improvement of sensitivity and reduction of self-absorption. The inter pulse delay and the energies of the laser pulses have great effects on the emission spectra. Therefore, in order to carry out the experiment the inter pulse delay and the energy ratio were optimized.

3.4.3 Inter pulse delay optimization

The inter pulse delay has been varied from 0 to 13 μs and the emission spectra have been recorded in steps of 1 μs. From the emission spectra, signal intensity of Ca (866.22 nm) and Zn (589.4 nm) lines have plotted as a function of inter pulse delay as shown in **Fig. 3.14.** This figure shows that the maximum signal intensity is at 8 μs inter pulse delay. Rizwan et al. [54] used Al and Mg lines and reported the maximum enhancement in signal intensity at 25 μs inter pulse delay, and Colao et al. [59] optimized the signal of the aluminum target at inter pulse delay of 40 μs. Killinger et al. [60] performed their work on the ceramic alumina target with inter pulse delay of 0.2 μs up to 3μs. This literature survey show that inters pulse delay depends upon the nature of the target material and on the experimental conditions.

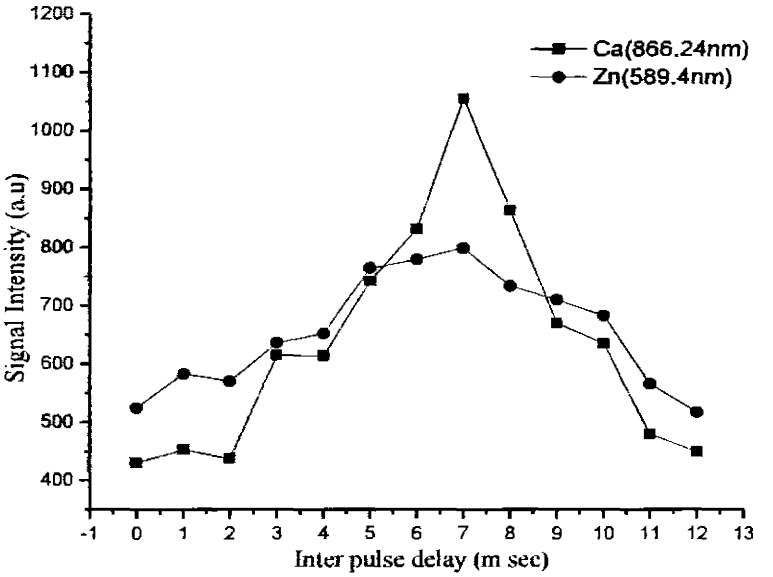

Figure 3.14 Plot of signal intensity versus interpulse delay of Ca (866.24 nm) and Zn (589.44 nm) lines.

Setting the inter pulse delay at 8 μs, the energy ratio of both the laser pulses was optimized for better and enhanced signal in the present experimental conditions. This was done by adjusting the pulse energies of both the lasers in such a way to get maximum signal intensity.

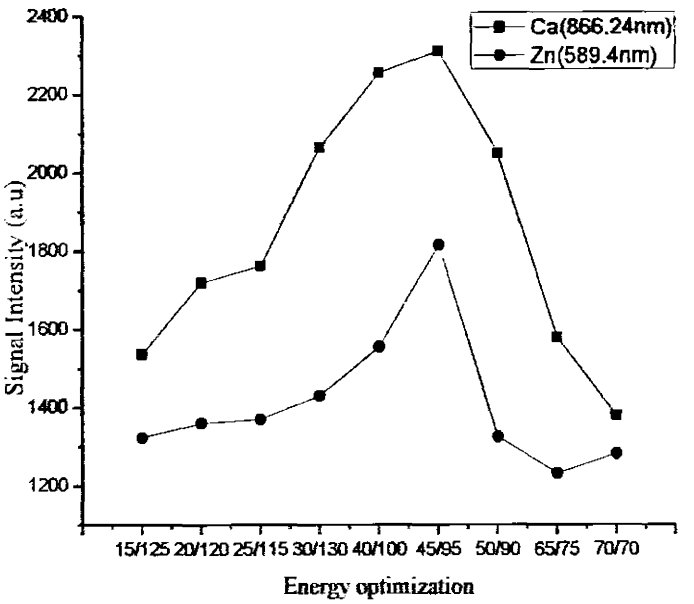

Figure 3.15 Energy optimization for double pulse.

The energies of the two lasers have been optimized as shown in **Fig 3.15.**The experiment was performed by using two lasers at 1064 nm with interpulse delay of 8μs. The energy ratio is varied from 15/125 mJ up to 70/70 mJ ($E_{1st\ laser}/E_{2nd\ laser}$) and signal intensity of Zn (589.4 nm) and Ca(866.22 nm) lines have been plotted. The plot shown in **Fig. 3.15** yield the maximum signal at the energy ratio of 45/95 recorded and as a function of energy ratio. This optimized signal is observed at 8 μs delay. Setting the interpulse delay at 8 μs and the energy ratio at 45/95 mJ the plasma has been generated on the turnip skin and central part recorded via LIBS2500+ spectrometer observed when the second laser pulse energy is two times of the first laser pulse. It is evident that for a better result of a DP LIBS, the energy of second laser pulse should be kept higher than the first one.

3.4.4 Comparison of Single and Double pulse

Utilizing the interpulse delay and energy settings, the DP LIBS spectra have been recorded under the same experimental condition as used for SP LIBS. As shown in **Fig. 3.16** shows that element Fe reveals 10 times signal enhancement.

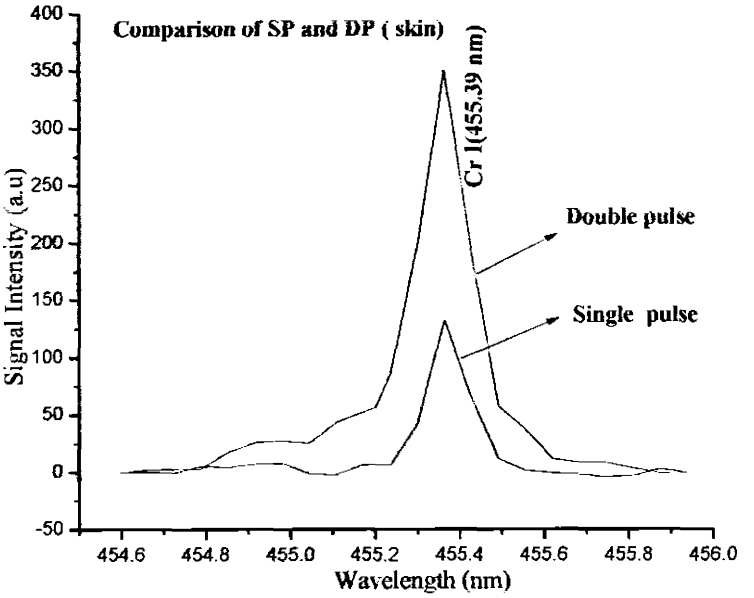

Figure 3.16 Comparison of intensities using single and double pulse on the skin of turnip.

Hence the double pulse spectrum clearly shows increase in emission intensities of as well as trace elements in turnip. The double pulse (DP) technique has proven its feasibility to increase the sensitivity of LIBS. Gautier C et al. [44] has demonstrated their work for the signal enhancements by using double pulse. Babushok VI et al. [61] has also proved that double pulse technique is a reliable method for intensity enhancements.

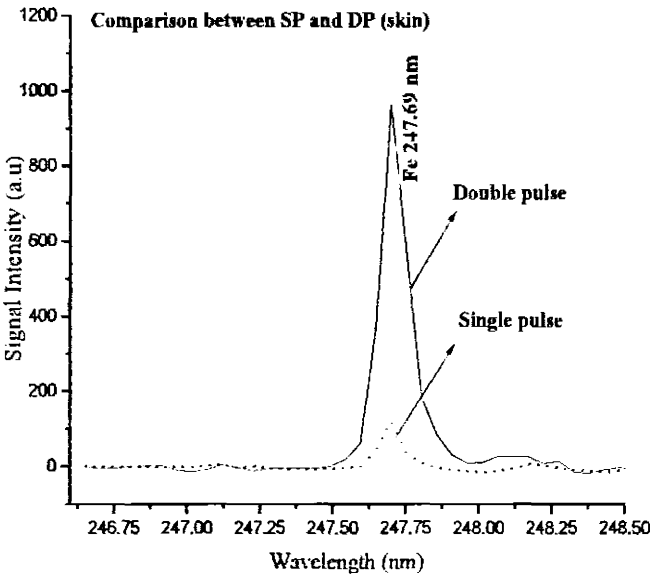

Figure 3.17 Comparison of single and double pulse for Fe I (247.69 nm).

The choice of observing the effects of double pulse on the skin was motivated due to presence of larger metal content as compared to the flesh of turnip [2] The larger the metal contents the more efficiently laser energy coupled to the sample, this causes detection of more atomic lines in emission spectra. S.beldjilali et al. [35] compared the single pulse and double pulse effects on potato skin. They investigated the improvement in plasma dynamics by the use of double pulse.

3.4.5 Space resolved analysis for Double pulse

This signal enhancement in double pulse LIBS motivated us to analyze the constituents of the turnip. For this purpose the double pulse emission spectra recorded at different locations from center to skin. As shown in **Fig 3.17** the double pulse spectra clearly show the increase in the emission intensities of major elements as well as trace elements.

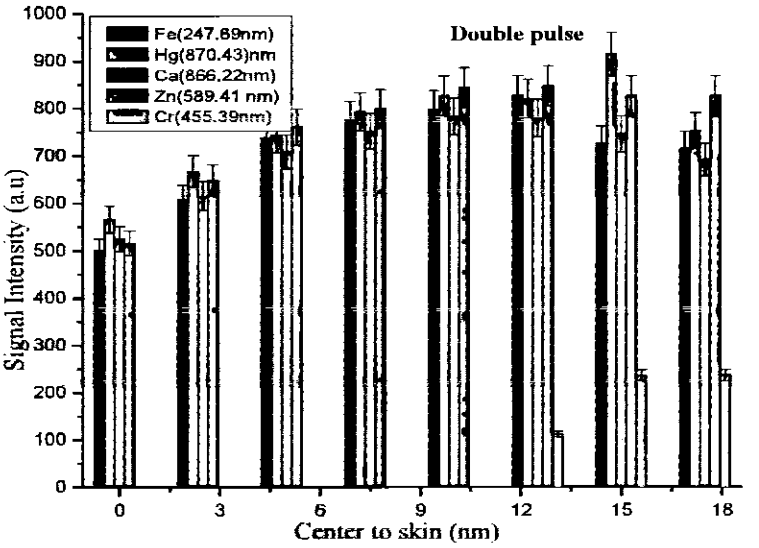

Figure 3.18 Spatial variation of selected heavy metals from center to skin.

It is observed that the concentration of trace elements is maximum at the skin and gradually decreases in the flesh of turnip. The same behavior has also been observed for single pulse LIBS, but with low intensities. The Cr has the least intensity and quickly decay in the inner part of the turnip. At half the way from the skin to center, Cr vanishes, this behavior of Cr is also observed in the Single pulse LIBS of turnip. Which shows that Cr has least penetration power. And Zn shows the highest penetration power as its concentration does not vary abruptly from center to skin.

It is evident from the **Figure 3.18** that Zn has same concentration up to middle of the turnip and then decreases. On the other hand Ca, Hg and Fe has relatively low concentration on the skin of turnip and just on the inner part of the skin. Therefore, its concentration increases up to 6 mm inside the turnip and again reduces up to the center of the turnip. The low concentration on the skin may be due to the reason that the turnip is washed with water which cleansthe surface up to some extent.

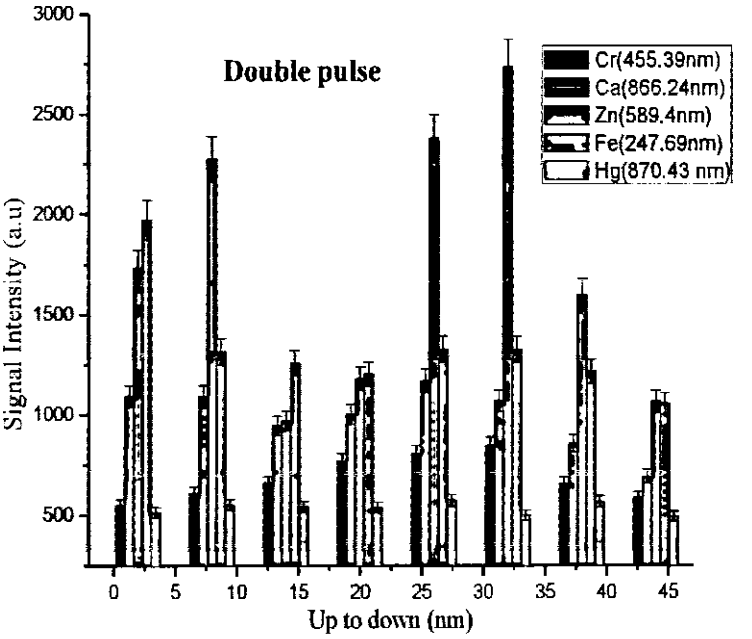

Figure 3.19 Comparison of signal heights of trace elements and main constituent of turnip in up to down profile.

As we have already discussed the variation of elemental concentration on the skin of turnip by using single pulse LIBS, we have repeated the experiment with double pulse LIBS under identical experimental conditions, to observe how double pulse affects the LIBS measurements. **Fig 3.19** demonstrated the variation of Cr, Ca, Zn, Fe and Hg as a function of distance from Up to down profile on the skin of the turnip. As shown, the top portion of the turnip has high contents of Zn, Fe, Ca, which decreases as we go towards the bottom of the turnip. However the location where it touches the soil (25 mm up to 33 mm) from the top, the concentration of above mentioned three elements again increases. When the portion inside the soil has been analyzed, it was observed that the concentration of Zn, Ca and Fe was not as high as on the surface. This may reduce seepage occurred in

the lower portion of the turnip, which results low concentration of these elements. Unlike these elements, Cr has less concentration at both upper and lower parts of turnip but it is maximum at that particular point where it just touches the soil. This can be concluded as, that Cr is present in high quantity at the soil surface but its transmission on the skin is very less.

Conclusion

We have performed spectroscopic analysis of the plasma produced by laser ablation of aluminum-alloy and steel alloys and on the skin and inner of the turnip using infrared radiation (1064 nm).

The qualitative analysis of the emission spectra of aluminum alloys and steel alloys confirm the presence of lowest concentration trace element, chromium, molybdenum respectively. This reveals the sensitivity and selectivity of the emission spectra, which has been further improved by the use of double pulse LIBS. The qualitative analysis of trace/heavy elements in turnip shows the presence of iron, calcium, mercury, zinc, and chromium. The chromium was found to have least signal intensity revealing that it has the lowest concentration element present in turnip. In addition, the electron temperature and electron number density were determined using Boltzmann plot method and stark broadened line profile of iron emission line respectively.

Future Recommendation

In future, we will extend this work towards the real time compositional and qualitative analysis in extreme environments likehigh temperature region and contaminated areas and apply the standoff capability to the inaccessible locations. Although LIBS is quite useful for elemental analysis, it is less for molecular analysis. As a result, studies combining LIBS and Raman will be much more useful for compositional and qualitative analysis of samples.

References

[1] B. Salle, P. Mauchien, S. Maurice, SpectrchimicaActa part B **62,** 739 (2007).

[2] S. Beldjilai, D. Borivent, L. Mercadier, E. Mothe , G. Clair , J. Hermann,Spectrchimica Acta part B **65,** 727 (2010).

[3] H. Moenke, M.Blankenburg, Laser Microspectral Analysis,Crane and Russak Company, Inc., 1973.

[4] F. Brech, L. Cross, Appl. Spectrosc. **16,** 59 (1962).

[5] D. J Guédon, , N. Liodec , C.R. Acad. Sci. **257**, 3336(1963).

[6] R. Tambay, R. Thareja, R.K., J. Appl. Phys., **70(5),** 2890(1991).

[7] S.R.J. Brueck, H.Kildal, J.Appl. Phys., **52**, 1004(1981).

[8] H. Busher, R.Thomlinsen, R. Damon, Phys. Rev. Lett., **15**, 847 (1965).

[9] A.J. Alcock., C.De Michelis, M.C. Richardson, Appl. Phy. Lett., **Vol. 15**, 72 (1969).

[10] W.Schroeder, J.J. van Niekirk, L. Dicks, A. Strashei, H.V.D. PiepenSpectrochim.Acta Part B **26**, 331 (1971).

[11] R.H Scott, and A. Strasheim , Spectrochim.Acta Part B **25**, 311(1970).

[12] D.A., Cremers, L.J. Radziemski, Anal.Chem. **55**, 1252(1983).

[13] L.J. Radziemski, Loree, T.R., Cremers, D.A., Hoffman, N.M., Anal.Chem. **55**, 1246 (1983)

[14] E.B. Belyaev, E.B., Godlevski, A.P., Kopytin, Y.D., Sov.J.Quant.Electron. **8**, 1459 (1978).

[15] J.R. Wachter, D.A.Cremer, Appl. Spect. **41**, 1042(1987).

[16] L.J. Radziemski, T.R. Loree, J. Plasma Chem. Plasma Proc. **1,**281 (1981)

[17] D.A. Cremers, L.J. Radziemski, Anal. Chem. **55,**1252 (1983).

[18] D.E. Poulain, D.R. Alexander, Appl. Spectrosc. **49,**569(1995).

[19] C. Aragon, J.A. Aguilera, J. Campos, Appl. Spectrosc. **47,** 606 (1993).

[20] J.A. Aguilera, C. Aragon, J. Campos, Appl. Spectrosc. **46**, 1382 (1992)

[21] Energy and Environment, Sandia Technology Bulletin, May 1994.

[22] M. Sabsabi, P. Cielo, Appl. Spectrosc. **49, 499** (1995).

[23] B.C. Castle, K. Talabardon, B.W. Smith, J.D. Winefordner , Appl. Spectrosc.**52** 649 (1998).

[24] Ciucci, M. Corsi, V. Palleschi, S. Rastelli, A. Salvetti,E. Tognoni, Appl. Spectrosc. **53**, 960 (1999).

[25] D.W. Hahn, and M.M. Lunden. Aerosol Science and Technology.**33**, 30 (2000).

[26] O. Samek, D.C.S. Beddows, J. Kaiser, S.V. Kukhlevsy, M. Liška, H.H. Telle, J. Young, Optical Engineering, **39**, 2248 (2000).

[27] M. Kraushaar, R. Noll and H.U. Schmitz, Applied Spectroscopy, **57**, 1282 (2000).

[28] P.L. García, J.M. Vadillo and J.J. Laserna Applied Spectroscopy, **58**,1347.

[29] D.A. Cremers, and L.J. Radziemski. Handbook of laser-induced breakdown spectroscopy. John Wiley & Sons, Ltd.(2006).

[30] N. Labbé, N., I.M. Swamidoss, N. André, M.Z. Martin, T.M. Young and T.G.Rials. Applied optics, **47,** 158.

[31] Vadillo, J.M., K. Cardell, D.A. Cremers and J.J. Laserna. **18**, 169 (1999).

[32] Sirven, J.B., B. Bousquet, L. Canioni, L. Sarger, S. Tellier, M. Potin-Gautier andI.L. Hecho, Analytical andBioanalytical Chemistry, **385**, 256 (2006).

[33] J. Kaise., O. Samek, L. Reale, M. Liška, R. Malina, A. Ritucci, A. Poma, A. Tucci, F. Flora, A. Lai, L. Mancini, G. Tromba, F. Zanini, A. Faenov, T. Pikuzand G. Cinque. Microscopy Research andTechnique **70,** 147 (2007).

[34] S. Darwiche,R. Benrabbah , M. Benmansour Daniel SpectrochimicaActa Part B **74,**115 (2012).

[35] S. Beldjilali, W. L. Yip, J. Hermann, T. Baba-Hamed, A. Belasri AnalBioanalChem.**400**, 2173 (2011).

[36] J. M. Gomba et al Spectrochimica Acta Part B **56**, 695 (2001).

[37] B. Le Dragoff, J. Margot, M. Chaker, M. Sabsabi, O. Barthelemy, T. W. Johnston, S. Laville, F. Vidal and Y. von Kaenel, Spectrochimica Acta Part B **56**, 987 (2001).

[38] L.I. Hong-Kun, L.I.U. Ming, C. Zhi-jiang, L.I. Run-Hua, Trans. Nonferrous Met.Soc. China.**18,** 222 (2008).

[39] Ernst and Wolfgang, Farson, Dave F, Sames, D. Jason, Appl. Spectrosc. **50**, 306(1996).

[40] Bassiotis, A. Diamantopoulou, A. Giannoudakos, F. Roubani-Kalantzopoulou, M. Kompitsas, Spectochmica Acta Part B **56**, 671 (2001).

[41] C. Lozep Moreno, K. Amponah-Manager, B. W. Smith, I. B. Gornushkin, N. Omenetto, S. Palanco, J.J. Laserna and J.D. Winefordner, J. Anal. At. Spectrom. **20**, 552 (2005).

[42] X. K. Shen, H. Wang, Z. Q. Xie, Y. Gao, H. Ling, and Y. F. Lu, Applied Optics.**48**, 2551 (2009).

[43] V. Juvé, R. Portelli, M. Boueri, M. Baudelet, J. Yu Spectrochimica Acta Part B **63**, 1047 (2008).

[44] C. Gautier, P. Fichet, D. Menut, J. L. Lacour, D. L'Hermite ,J. Dubessy SpectrochimActa B.**60**, 265 (2005).

[45] J. Scaffidi, J. Pender, W. Pearman, S.R. Goode, B.W. Colston Jr, J.C. Varter, S.M. Angel Appl Opt.**42**, 6099 (2003).

[46] V.N. Rai, F.Y. Yueh, J.P. Singh, Appl Opt.**42**, 2085 (2009).

[47] S. N Thakur and J. P Singh, Laser induced breakdown spectroscopy, Elsevie(2007).

[48] C. E. Moore, Selected Tables of Atomic Spectra, Washington, N.S.R.D.S.-N.B.S. 3, Section 1 (1965) and Section 2 (1967)

[49] C. E. Moore, Bibliography on the Analysis of Optical Atomic Spectra, Section 1, H toV, N.B.S. Special Publ. 306, Washington (1968)

[50] http://www.physics.nist.gov/PhysRefData/ASD/lines_form.html NIST, National Institute of Standards and Technology for the United States of America.

[51] http://www.arl.army.mil/www/default.cfm?Action=247&Page=250 ARL, US Army Research Laboratory.

[52] D.A. Cremers, L.J. Radziemski, T.R. Loree, Appl Spectrosc **38,** 721 (1984)

[53] J. Uebbing, J. Brust, W. Sdorra, F. Leis and K. Niemax,Appl. Spectrosc.**45,** 1419 (1991).

[54] Rizwan Ahmed , M. Aslam baig, Journal of Applied physics **106**, 033307 (2009)

[55] Kuwako A, Uchida Y, Maeda K. Appl Opt. **42**, 6052 (2003).

[56] Q.J. Guo, H.B. Yu HB, Y. Xin, X.L. Li, X.H. Li Society of Applied Spectroscopy**30,** 783 (2010).

[57] W. Lei, V. Motto-Ros , M. Boueri Q. Ma, D. Zhang. L. Zheng , H. Zen, J. Yu, Spectrochim Acta B **64,** 891 (2009).

[58] F. Colaoa,, V. Lazica, R. Fantonia, S. Pershin Spectrochimica Acta Part B **571**167 (2002).

[59] D. K. Killinger, D.A. Susan, D.W. Robert, S. Chris Stefano, L.D. Edwin Opt. Express **15,** 12905 (2007)

[60] V.I. Babushok, F.C. DeLucia Jr, J.L. Gottfried , C.A. Munson , A.W. MiziolekSpectrochim Acta B **61** ,999 (2006)

[61] A.W. Miziolek, V. Palleschi, I. Schechter I, Cambridge University Press, Cambridge (2006).